iScience

CellPress
OPEN ACCESS

Article

Artificial antigen-presenting cell system reveals CD28's role in modulating T cell functions during human immunodeficiency virus infection

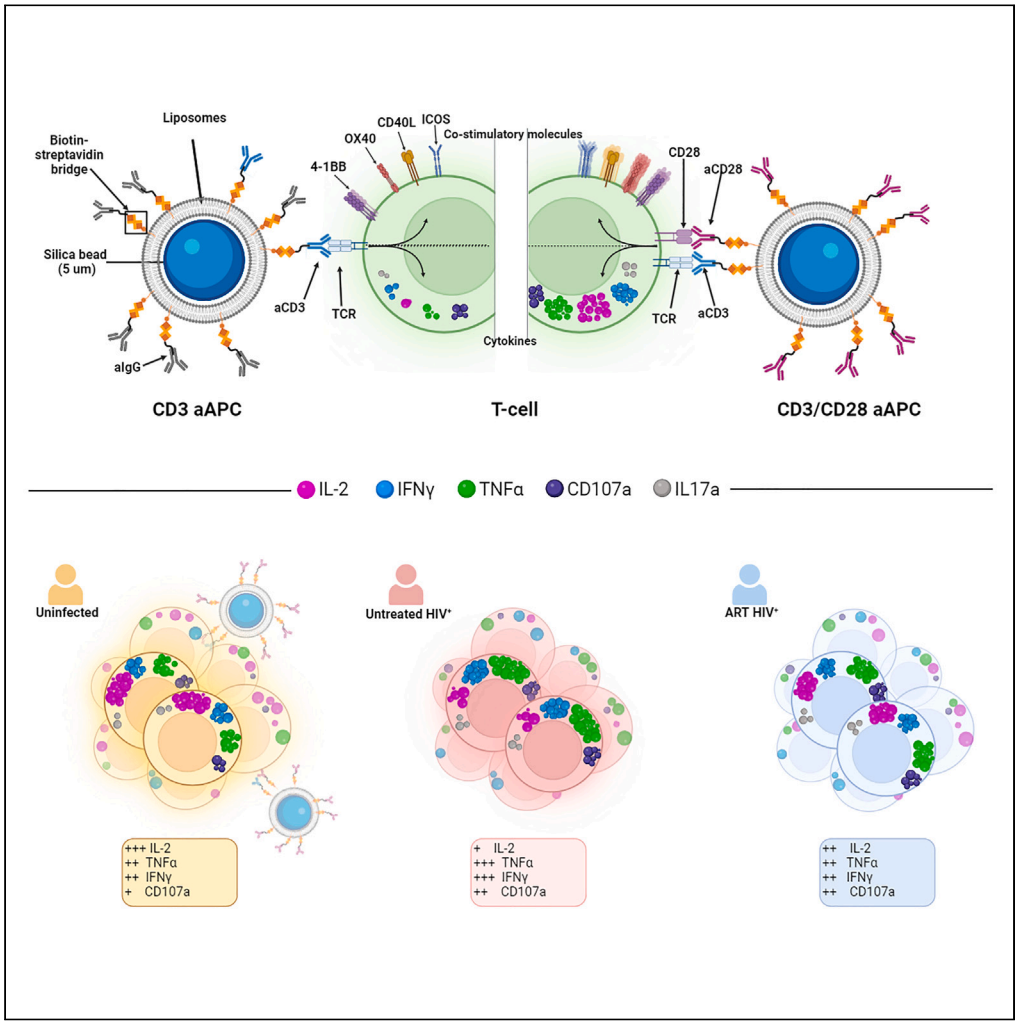

Tayma Shaaban Kabakibo, Edwige Arnold, Kartika Padhan, ..., Naglaa Shoukry, Mathieu Dubé, Daniel E. Kaufmann

mathieu.dube.chum@ssss.gouv.qc.ca (M.D.)
daniel.kaufmann@chuv.ch (D.E.K.)

Highlights

The aAPC system induces robust cytokine production in CD4$^+$ and CD8$^+$ T cells

CD28 co-stimulation enhances T cell function in a cytokine-dependent manner

Untreated people with HIV show skewed functions: increased TNFα and reduced IL-2

Antiviral therapy partially corrects dysfunction in CD4$^+$, but not in CD8$^+$ T cells

Kabakibo et al., iScience 27, 110947
October 18, 2024
https://doi.org/10.1016/j.isci.2024.110947

iScience

CellPress
OPEN ACCESS

Article

Artificial antigen-presenting cell system reveals CD28's role in modulating T cell functions during human immunodeficiency virus infection

Tayma Shaaban Kabakibo,[1,2,3] Edwige Arnold,[1,2] Kartika Padhan,[1,8] Audrée Lemieux,[1,2,3] Gloria Gabrielle Ortega-Delgado,[1] Jean-Pierre Routy,[5,6] Naglaa Shoukry,[1,2,4] Mathieu Dubé,[1,*] and Daniel E. Kaufmann[1,2,4,7,9,*]

SUMMARY

T cell immune dysfunction is a prominent feature of chronic HIV infection. To evaluate non-specific dysfunction, a method involving both generic activation and T cell receptor (TCR) stimulation is necessary. We created a tunable artificial antigen-presenting cell (aAPC) system. This system consists of lipid bilayers on cytometry-compatible silica microbeads (5 μm). When only anti-CD3 is incorporated, T cell activation is limited. Introducing anti-CD28 agonists significantly elevates the cytokine expression and upregulation of activation-induced markers. CD28 co-stimulation modulates the response profile, preferentially promoting IL-2 expression relative to other cytokines. aAPCs-stimulated CD4$^+$ and CD8$^+$ T cells from untreated HIV-infected individuals exhibit altered effector functions and diminished CD28 dependence. These functions are skewed toward TNFα, IFNγ and CD107a, with reduced IL-2. Antiretroviral therapy partially normalizes this distorted profile in CD4$^+$ T cells, but not in CD8$^+$ T cells. Our findings show T cell intrinsic biases that may contribute to persistent systemic T cell dysfunction associated with HIV pathogenesis.

INTRODUCTION

Optimal T cell activation requires two signals delivered during the interaction between T cells and antigen-presenting cells (APCs). Signal 1 occurs when the T cell receptor (TCR) binds to its cognate antigen presented on a major histocompatibility complex (MHC) class I or class II molecule. Signal 2 is provided by co-stimulatory molecules on T cells, which are engaged by their APC-expressed ligands.[1,2] The CD28-B7 axis is the most extensively studied co-stimulatory pathway (reviewed in[3,4]). The combined effects of signals 1 and 2 activate transcriptional factors governing various "differentiation programs," each defining a set of functions, such as T cell proliferation and survival, cytokine production, or differentiation.[5–8] It is now evident that the role of CD28 extends beyond enhancing TCR signaling, as it induces distinct transcriptional and epigenetic changes.[9–11]

Systemic chronic activation is a hallmark of progressive HIV infection.[12,13] Prolonged exposure to HIV peptides leads to the dysregulation of HIV-specific CD4$^+$ and CD8$^+$ T cells, altering T cell polarization and effector functions.[14–22] These dysfunctional responses usually fail to control viral replication.[22,23] T cell exhaustion is associated with persisting expression of immune checkpoint inhibitory receptors (IR), which exert negative feedback control on the TCR signal.[23–25] Modulation of CD28 activity plays a pivotal role in this negative feedback loop, as PD-1-associated SHP-2 preferentially dephosphorylates the cytosolic domain of CD28.[26] A broader state of T cell dysfunction also exists in non-HIV-specific cells, attributed to systemic activation,[27,28] co-infection by other pathogens,[29–31] and microbial translocation caused by compromised mucosal barrier integrity.[32] This generic dysfunction may contribute to co-morbidities and reduced life expectancy in people with HIV (PWH).[33] While decreased expression of CD28 on CD8$^+$ T cells is inversely correlated with CD4$^+$ T cell count prior to ART initiation,[34] it remains uncertain whether this overall dysfunction is associated with modified responsiveness to TCR and CD28 stimulation.

Stimulation with cognate antigenic peptides loaded onto natural APCs is commonly used to study TCR-mediated T cell functions. This approach provides insights into T cells sharing a defined specificity, but it does not provide information about the overall state of T cells. Furthermore, as natural APCs express an array of other co-stimulatory and inhibitory receptors, simplified model systems are needed to

[1]Research Centre of the Centre Hospitalier de l'Université de Montréal (CRCHUM), Montréal, QC, Canada
[2]Université de Montréal, Montréal, QC, Canada
[3]Département de Microbiologie, Infectiologie et Immunologie, Université de Montréal, Montréal, QC H2X 0A9, Canada
[4]Département de Médecine, Université de Montréal, Montréal, QC H2X 0A9, Canada
[5]Chronic Viral Illnesses Service and Division of Hematology, McGill University Health Centre, Montreal, QC H4A 3J1, Canada
[6]Infectious Diseases and Immunity in Global Health Program, Research Institute, McGill University Health Centre, Montreal, QC, Canada
[7]Division of Infectious Diseases, Department of Medicine, Lausanne University Hospital (CHUV) and University of Lausanne, Lausanne, Switzerland
[8]Present address: Center for Advanced Tissue Imaging, National Institute of Allergy and Infectious Disease, National Institutes of Health, Bethesda, MD, USA
[9]Lead contact
*Correspondence: mathieu.dube.chum@ssss.gouv.qc.ca (M.D.), daniel.kaufmann@chuv.ch (D.E.K.)
https://doi.org/10.1016/j.isci.2024.110947

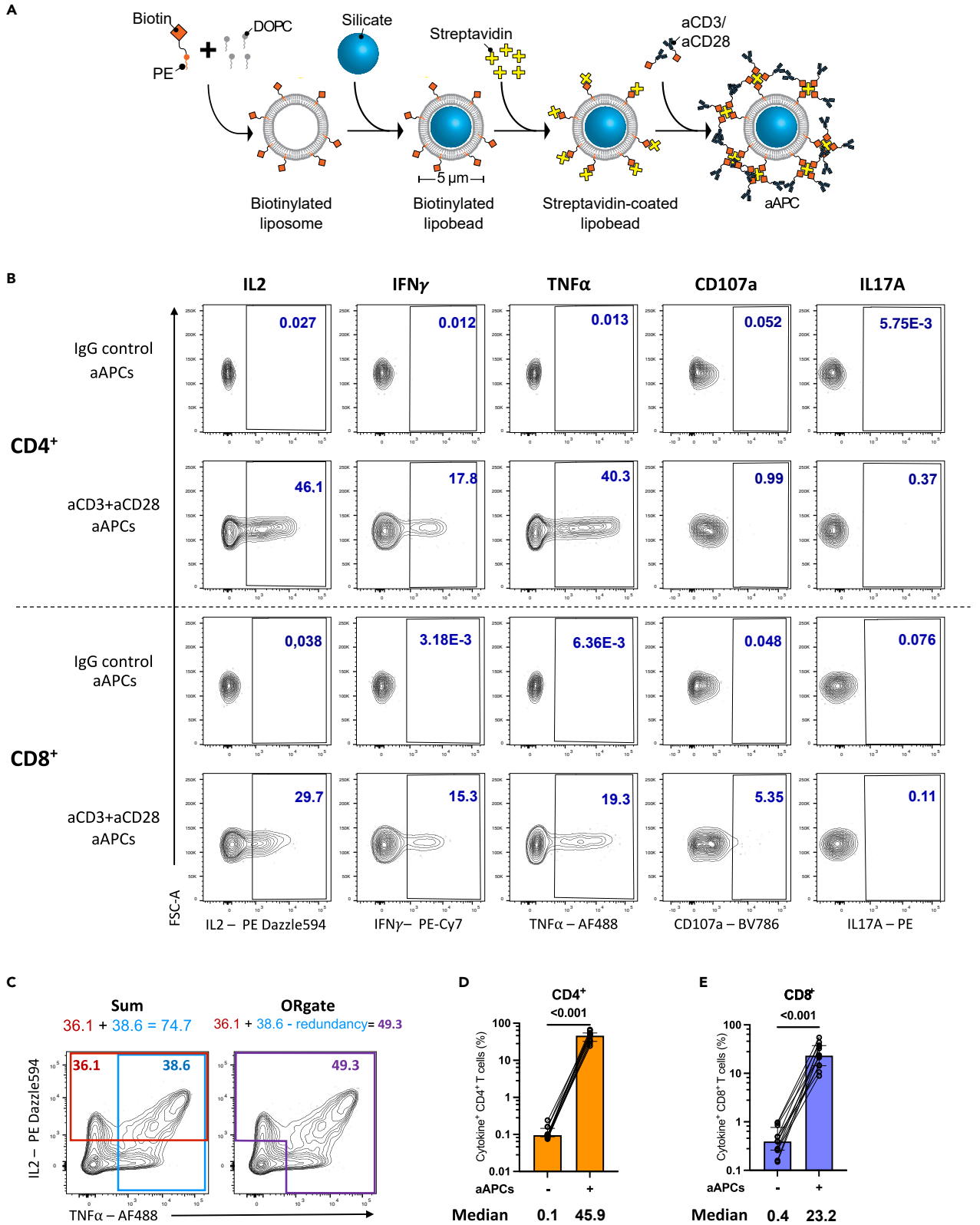
A
Biotin
PE
DOPC
Silicate
Streptavidin
aCD3/
aCD28
5 µm
Biotinylated
liposome
Biotinylated
lipobead
Streptavidin-coated
lipobead
aAPC
B
IL2
IFNγ
TNFα
CD107a
IL17A
IgG control
aAPCs
CD4+
aCD3+aCD28
aAPCs
0.027
0.012
0.013
0.052
5.75E-3
46.1
17.8
40.3
0.99
0.37
IgG control
aAPCs
CD8+
aCD3+aCD28
aAPCs
0,038
3.18E-3
6.36E-3
0.048
0.076
29.7
15.3
19.3
5.35
0.11
FSC-A
IL2 – PE Dazzle594
IFNγ– PE-Cy7
TNFα – AF488
CD107a – BV786
IL17A – PE
C
Sum
36.1 + 38.6 = 74.7
ORgate
36.1 + 38.6 - redundancy= 49.3
36.1
38.6
49.3
IL2 – PE Dazzle594
TNFα – AF488
D
CD4+
<0.001
Cytokine+ CD4+ T cells (%)
aAPCs
Median 0.1 45.9
E
CD8+
<0.001
Cytokine+ CD8+ T cells (%)
aAPCs
Median 0.4 23.2

Figure 1. aAPCs induce a robust cytokine production in CD4$^+$ and CD8$^+$ T cells

(A) Schematic representation of aAPCs preparation.

(B) Representative flow cytometry plots of cytokines expression in CD4$^+$ and CD8$^+$ T cells after 15h of aAPCs (aCD3:aCD28:IgG 1:4:0) stimulation of purified T cells from UD. The unstimulated condition represents T cells incubated with control IgG aAPCs (aCD3:aCD28:IgG 0:0:5).

(C) Diagram explaining the OR Boolean gating. For simplicity, only IL-2 and TNFα in CD4$^+$ T cells are shown as a conceptual example.

(D and E) Total cytokine$^+$ (D) CD4$^+$ or (E) CD8$^+$ T cells defined by the ORgate, in 12 UD. Wilcoxon test results are shown. Medians are indicated below the graphs. Error bars represent the interquartile range.

accurately analyze TCR- and CD28-mediated activation. Agonistic anti-CD3 (aCD3) and anti-CD28 (aCD28) antibodies are commonly used to non-selectively activate purified T cells, mimicking TCR and co-stimulation signals, respectively. Commercially available activation systems include crosslinked soluble aCD3 and aCD28 or immobilization of at least one of the antibodies on either plate-, planar-, or bead-based solid supports.[35–40] Previous studies indicated that having cell-sized constructs (4.5–5 μm)[41,42] and a fluid surface allowing the rearrangement of T cell ligands on the artificial APC (aAPC)[43,44] leads to enhanced T cell activation. Current embedded agonists on supported lipid membranes were effective for expanding T cells, but required days of stimulation, which complicates phenotyping.[45–49]

In this study, we developed a customizable artificial antigen-presenting cells (aAPCs) system composed of a fluid lipid bilayer coated onto cytometry-compatible silica microbeads (5 μm) and embedded with agonistic antibodies directed against CD3 and CD28. This system enables strong T cell activation within 15 h. We employed these aAPCs to elucidate the role of CD28 co-stimulation in shaping the CD4$^+$ and CD8$^+$ T cell effector functional profile in uninfected control donors (UD). We investigated how this profile changes in PWH, both before (UNT) and after antiretroviral treatment (ART).

RESULTS

Artificial antigen-presenting cells induce robust cytokine production in CD4$^+$ and CD8$^+$ T cells

We developed a T cell activation system consisting of silica beads coated with a membrane bilayer to mimic the physiological TCR-mediated T cell activation. This design imitates key features of natural APCs including a similar size (5 μm diameter), a tridimensional structure, and a fluid lipid bilayer that facilitates the clustering of activating ligands. As "artificial antigen-presenting cells (aAPCs)" was a term previously used to describe such a three-dimensional system replicating some aspects of natural APC-mediated activation, we adopted this expression herein for our newly designed activation platform.[50,51] The preparation of aAPCs (Figure 1A) involved generating unilamellar liposomes containing biotin acceptor sites through thin film hydration. Bilayered liposomes were formed by extrusion and used to coat the silica beads. Biotin-conjugated anti-CD3 and/or anti-CD28 agonistic antibodies were added via streptavidin-biotin ligation.

We assessed the potency of aAPCs at stimulating CD4$^+$ and CD8$^+$ T cells isolated from PBMCs of uninfected donors (UD, Table S1). Following purification, T cells were stimulated for 15h with aAPCs coated with aCD3 and aCD28 antibodies at a 4:1 bead-to-cell ratio. Subsequently, an intracellular cytokine staining assay (ICS) was conducted to detect IL-2, IFNγ, TNFα, CD107a, and IL17A. The aAPCs were co-analyzed alongside the T cells (Figure S1A). The successful coating with aCD3 and aCD28 antibodies was verified through anti-IgG staining (Figure S1B). Upon stimulation with aAPCs, a considerable upregulation of cytokines was observed in both CD4$^+$ and CD8$^+$ T cells (Figure 1B). IL17A was not detectable in CD8$^+$ T cells and was consequently excluded from subsequent CD8 analyses (Figure 1B). The extent of activation achieved through aAPCs was close to the level attained through the superantigen staphylococcal enterotoxin B (SEB) (Figure S1C). Of note, SEB-mediated activation was performed in non-purified PBMCs to adequately cross-link MHC-II and TCR molecules and ensure superior activation (Figure S1D).

We assessed the frequencies of CD4$^+$ and CD8$^+$ T cells expressing at least one cytokine. Each cytokine was individually gated, then subjected to ORgate Boolean gating.[52] This approach creates a cytokine$^+$ population that includes all cells within IL-2$^+$, IFNγ$^+$, TNFα$^+$, CD107a$^+$ gates. Additionally, the use of the ORgate Boolean gating prevents the redundant counting of cells that simultaneously co-express several effector molecules, which would otherwise occur with a simple summation (Figure 1C). This approach preserved all the possible cytokine combinations, such as single positive cytokine$^+$ cells as well as cell positives for several or all cytokines. Employing this strategy, we determined that a median of 45.8% of CD4$^+$ and 22.9% of CD8$^+$ T cells exerted $\geq$ 1 effector functions upon activation by aAPCs (Figures 1D and 1E). The embedding of antibodies into the lipid-bilayered silica bead was important, given that equivalent concentrations of aCD3 and aCD28 in solution or cross-linked with goat anti-mouse IgG only yielded low activation of CD4$^+$ and CD8$^+$ T cells (Figure S1E). We also compared our system to commercially available magnetic CD3$^+$CD28 beads (Figure S1F). Although magnetic bead-mediated stimulation appeared twice more efficient when gated on valid events, it came at the expense of an alteration of some cell surface marker expression, much higher cell death, and drastically inferior yield of T cell recuperation after stimulation (Figures S1G–S1I). By comparison, aAPCs provided a robust activation signal that nevertheless preserved cell viability and surface CD4 and CD8 expression (Figures S1J and S1K). The engagement of CD3 and CD28 with their agonistic antibodies resulted in their partial downregulation from the surface of both CD4$^+$ and CD8$^+$ T cells owing to strong stimulation cues (Figures S1J and S1K).

These data show that our devised aAPC system, utilizing silica bead-coated bilayers to emulate physiological TCR-mediated activation, robustly induces cytokine expression in both CD4$^+$ and CD8$^+$ T cells while preserving the viability of the cells.

CD28 co-stimulation differentially enhances individual effector functions in CD4$^+$ and CD8$^+$ T cells

We employed aAPCs to analyze the quantitative contributions of aCD3 and aCD28 to T cell activation. To empirically establish the optimal aCD3/aCD28 ratio in the aAPC system, we initially conducted dose-response experiments (Figures S2A and S2B). Increasing the

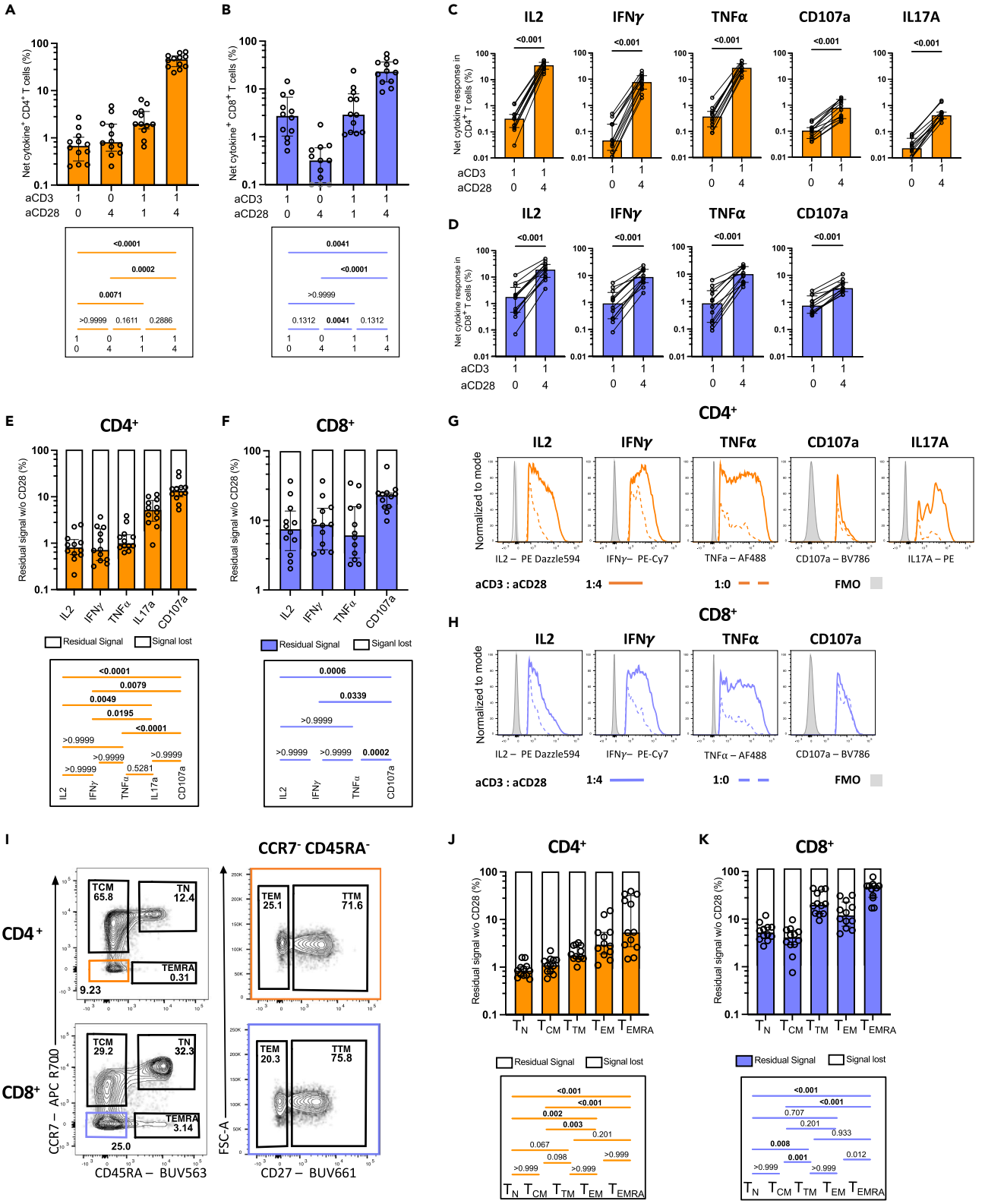
A
B
C
IL2
IFNγ
TNFα
CD107a
IL17A
D
E
CD4+
F
CD8+
G
H
I
CCR7- CD45RA-
J
K
Residual Signal
Signal lost
aCD3 : aCD28
1:4
1:0
FMO

Figure 2. CD28 co-stimulation differentially enhances effector functions in T cells

Univariate analyses of cytokine expression in $CD4^+$ and $CD8^+$ T cells after 15h of aAPCs stimulation of purified T cells from UD participants. Unless specified otherwise, the 1:4:0 (aCD3:aCD28:IgG) is presented.

(A–D) ORgate-identified net $cytokine^+$ responses after background subtraction. Net ORgate $cytokine^+$ (A) $CD4^+$ and (B) $CD8^+$ T cells responses to aAPCs stimulation with different aCD3:aCD28 ratios in purified T cells. Individual net cytokine production in (C) $CD4^+$ and (D) $CD8^+$ T cells when stimulated with aCD3 aAPCs (aCD3:aCD28:IgG 1:0:4) compared to aCD3+aCD28 aAPCs (aCD3:aCD28:IgG 1:4:0). Wilcoxon test results are shown.

(E and F) Percentage of residual $cytokine^+$ signal, representing the quotient between the 1:0:4 (aCD3:aCD28:IgG) and 1:4:0 (aCD3:aCD28:IgG) conditions in (E) $CD4^+$ and (F) $CD8^+$ T cells.

(G and H) Median fluorescence intensity (MFI) of each cytokine expression in (G) $CD4^+$ and (H) $CD8^+$ T cells when stimulated with aCD3 aAPCs (aCD3:aCD28:IgG 1:0:4) compared to aCD3+aCD28 aAPCs (aCD3:aCD28:IgG 1:4:0). The analyses focus the $cytokine^+$ cells indicated by the subtitles.

(I) Gating strategy defining memory subsets. The populations boxed in colors were further analyzed for CD27 expression, on the right.

(J-K) Percentage of residual ORgate $cytokine^+$ signal in $CD4^+$ and $CD8^+$ memory subsets (as calculated in E,F). In (A–F, J and K), $n = 12$. Friedman test was used in (A, C, E, F, J, K). In (A–F, J, and K), error bars represent the interquartile range.

concentration of aCD28 on aAPCs did not compensate for the absence of aCD3. In the absence of aCD28, increasing the aCD3 concentration had little effect, suggesting that CD28 co-stimulation is necessary for optimal activation. In the presence of aCD28, a high concentration of aCD3 proved detrimental. The optimal activation was empirically determined to be at a 1-to-4 aCD3-to-aCD28 molecular ratio. This ratio was selected for subsequent experiments unless otherwise specified.

To evaluate the importance of CD28 co-stimulation for distinct effector functions, we generated 5 sets of aAPCs: 1) negative control lipobeads loaded with non-activating isotype control IgG, and aAPCs containing agonistic antibodies targeting 2) CD3 only, 3) CD28 only, 4) CD3 and CD28 at equivalent but suboptimal molarity, and 5) CD3 and CD28 at the optimal 1-to-4 molecular ratio. Isotype IgG was supplemented onto suboptimal aAPCs to reach an overall antibody density equivalent to that of the optimal 1-to-4 condition. Purified T cells from 12 UD were stimulated with these sets of aAPCs, and total frequencies of cytokine-producing cells were quantified using OR Boolean combination gating (Figures S2C and S2D). Net total responses were calculated after subtracting the background signal (Figures 2A–2D).

In $CD4^+$ T cells, activation with aCD3 alone or aCD28 alone resulted in net responses of low magnitude (Figure 2A), which were still significant compared to negative IgG bead controls (Figure S2C). The signal modestly increased at the suboptimal 1:1 aCD3:aCD28 ratio, and substantially augmented at the optimal 1:4 (aCD3:aCD28) ratio, reaching a 69-fold rise compared to aCD3 alone. Compared to $CD4^+$ T cells, aCD3 alone was slightly more effective in activating $CD8^+$ T cells (Figure 2C). The benefit of co-stimulation was apparent only at the 1:4 M ratio, with a median-fold increase of 9.6 when compared to aCD3 alone. Positive impacts of CD28 co-stimulation were observed for each examined cytokine in both $CD4^+$ and $CD8^+$ T cells (Figures 2B and 2D).

To better illustrate the effect of CD28 co-stimulation on effector functions at the populational level, we calculated the residual signal in the absence of CD28 co-stimulation: ([$cytokine^+$ cells activated by aCD3 alone]/[$cytokine^+$ cells activated by 1:4 (aCD3:aCD28)] X 100) (Figures 2E and 2F). A low residual signal indicates a high dependence on CD28 co-stimulation, whereas a comparatively high residual signal suggests a certain degree of independence from CD28 co-stimulation. These internally controlled side-by-side comparisons allow the ranking of cytokines based on their dependence on CD28. In $CD4^+$ T cells, the expression of IL-2, IFNγ, and TNFα was markedly reduced without CD28. In contrast, IL17A and CD107a were less affected by the lack of CD28 co-stimulation (Figure 2E). CD28 co-stimulation dependency was more heterogeneous in $CD8^+$ T cells. Although a similar hierarchy existed, $CD8^+$ T cells depended less on CD28 co-stimulation than $CD4^+$ T cells for all effector functions, except CD107a (Figure S2E).

CD28 co-stimulation also increased cytokine expression at the single-cell level. Median fluorescence intensities of IL-2, IFNγ, TNFα, and IL17A all increased in the 1:4 (aCD3:aCD28) condition compared to aCD3 alone (Figures 2G, 2H, S2F, and S2G). Notably, only the expression of CD107a remained unchanged in $CD4^+$ and $CD8^+$ T cells. These data show the critical importance of CD28 to fully express cytokines.

Effector functions elicited in $CD4^+$ and $CD8^+$ T cells can vary with memory differentiation.[53,54] We, therefore, investigated whether this variability could lead to differing dependence on CD28 co-stimulation. Memory subsets were categorized as follows: naive T cells (T_N, $CCR7^+CD45RA^+$), central memory (T_{CM}, $CCR7^+CD45RA^-$), transitional memory (T_{TM}, $CCR7^-CD45RA^-CD27^+$), effector memory (T_{EM}, $CCR7^-CD45RA^-CD27^-$), and terminally differentiated memory (T_{EMRA}, $CCR7^-CD45RA^+$) (Figure 2I). There were no disparities in memory subset proportions after stimulation with aCD3+aCD28 aAPCs (Figures S2H and S2I). We evaluated total $cytokine^+$ cells in each subset using OR Boolean combination gating, then calculated the residual signal in the absence of CD28 co-stimulation (Figures 2J and 2K). In $CD4^+$ T cells, T_N exhibited the greatest reliance on CD28 co-stimulation. Across $CD4^+$ T memory subsets, we observed a hierarchy for dependence on CD28, wherein the need for co-stimulation diminished as subsets became more differentiated: $T_N > T_{CM} > T_{TM} > T_{EM} > T_{EMRA}$ (Figure 2J). $CD8^+$ T cell subsets displayed a three-step hierarchy in which T_N and T_{CM} were both strongly reliant on CD28, whereas T_{TM} and T_{EM} and moderately dependent on CD28. As for $CD4^+$ T cells, CD8 TEMRA were the least dependent on CD28. CD8 T cells required less co-stimulation overall than CD4 (Figures 2K and S2J). We tested whether independence from CD28 co-stimulation was linked to decreased CD28 expression in certain memory subsets. We observed that CD28 was expressed in more than 99% of T_N, T_{EM}, T_{TM} and T_{EM} CD4 T cell subsets. This proportion dropped to a still high median of 82.5% in TEMRA. There was more variation among subsets in CD8 T cells, with the highest proportion of $CD28^+$ in T_{CM} (median of 100%) and lowest in TEMRA cells (median of 36.6%) (Figure S2K). We next measured the median fluorescence intensity to infer the level of surface CD28 expression per $CD28^+$ cell (Figure S2L). The level of surface CD28 expression was similar across the differentiated subsets (T_{EM}, T_{TM}, T_{EM} and T_{EMRA}), and slightly lower in CD4 and CD8 T_N (Figure S2M). Importantly, T_{CM} had the same proportion of $CD28^+$ cells, and expressed the same level of surface CD28 compared to the least CD28 dependent T_{EM} in both CD4 and CD8

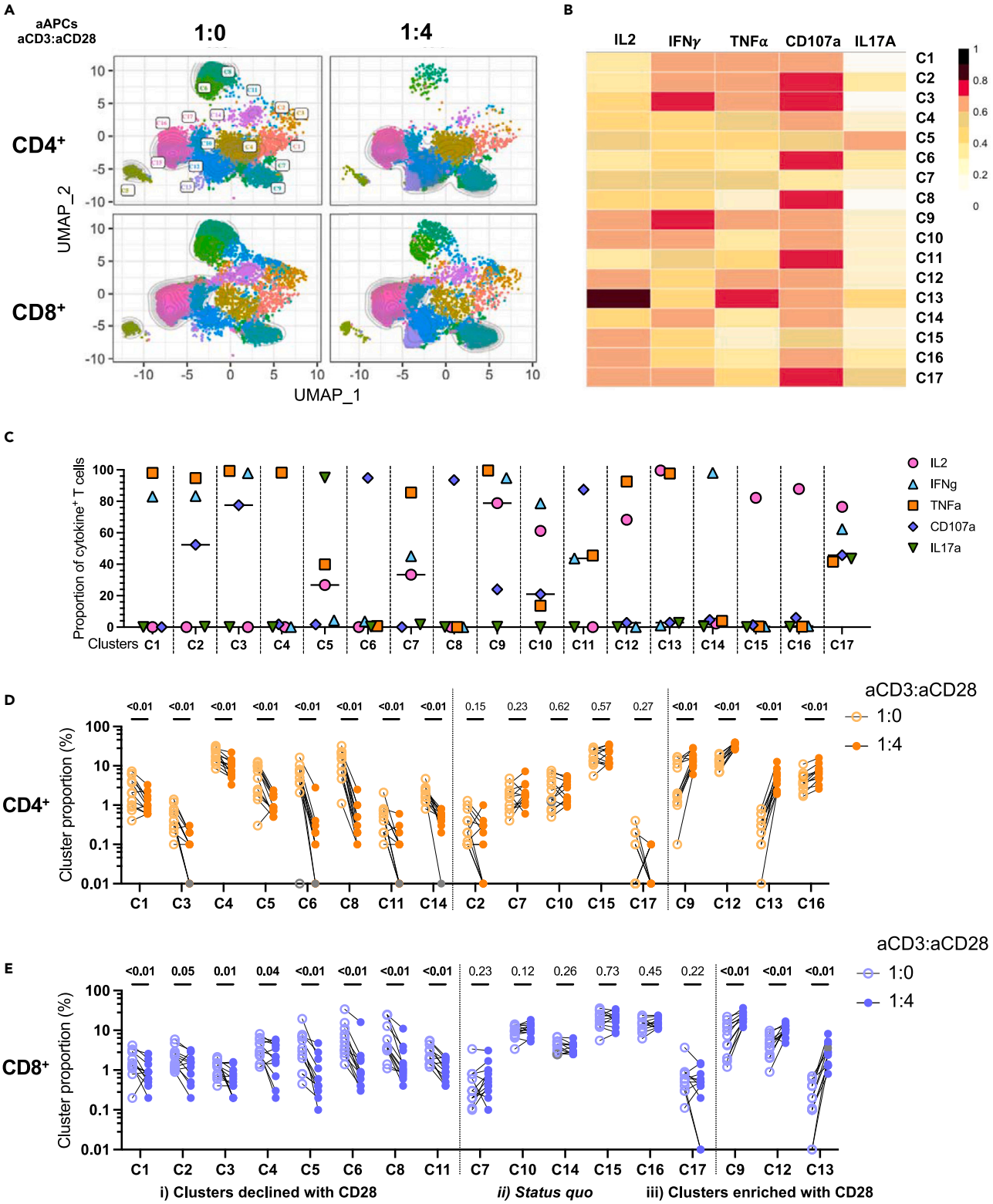
A
aAPCs
aCD3:aCD28
1:0
1:4
CD4+
CD8+
UMAP_2
UMAP_1
B
IL2
IFNγ
TNFα
CD107a
IL17A
C1
C2
C3
C4
C5
C6
C7
C8
C9
C10
C11
C12
C13
C14
C15
C16
C17
C
Proportion of cytokine+ T cells
Clusters
IL2
IFNg
TNFa
CD107a
IL17a
D
CD4+
Cluster proportion (%)
aCD3:aCD28
1:0
1:4
E
CD8+
Cluster proportion (%)
aCD3:aCD28
1:0
1:4
i) Clusters declined with CD28
ii) Status quo
iii) Clusters enriched with CD28

Figure 3. Responsiveness of IL-2 to CD28 co-stimulation shapes the effector profile

Multivariate analyses of cytokine expression in $CD4^+$ and $CD8^+$ T cells after 15h of aAPCs stimulation of purified T cells from UD participants. The 1:4:0 (aCD3:aCD28:IgG) and 1:0:4 (aCD3:aCD28:IgG) are herein qualitatively compared. $Cytokine^+$ CD4 and CD8 T cells are identified by Boolean ORgate gating, downsampled to 1000 cells per participant per condition, concatenated, and then analyzed as follows.

(A) Multiparametric UMAP representation of $cytokine^+$ $CD4^+$ and $CD8^+$ activated T cells from UD, based on IL-2, IFNγ, TNFα, CD107a and IL17A expression at two stimulation conditions (aCD3:aCD28:IgG): 1:0:4 and 1:4:0. The categorical $CD4^+$ and $CD8^+$ phenotypic information was reintroduced *post-hoc*.

(B) Heatmap summarizing the MFI of each parameter for each cluster.

(C) Proportion of cells expressing individual functions in each cluster, using the ORgate as the denominator and combining CD4 and CD8 T cells irrespective of the condition of stimulation; in support of panel B.

(D and E) Proportion of each $cytokine^+$ cluster for (D) $CD4^+$ and (E) $CD8^+$ T cells in uninfected participants. Wilcoxon paired tests are shown to depict the relative changes in cluster composition upon CD28 co-stimulation, compared to aCD3 alone. In (A–E), $n = 12$.

T cells. Therefore, independence from CD28 co-stimulation cannot be solely attributed to a lack of CD28 expression in certain differentiated subsets.

These results demonstrate the substantial impact of CD28 co-stimulation on the enhancement of T cell effector functions across $CD4^+$ and $CD8^+$ subsets, underscoring the differential dependence on CD28 co-stimulation across varying memory differentiation stages.

The heightened responsiveness of IL-2 to CD28 co-stimulation shapes the overall effector profile

Given the asymmetric impact of CD28 co-stimulation on cytokine expression, we investigated whether CD28 could act as a determinant shaping the overall effector profile. To avoid predefined marker combinations, we conducted unsupervised analyses utilizing the high-dimensional flow cytometric phenotyping data (Figure 3). We examined cells activated with different aCD3:aCD28:IgG ratios (1:0:4 vs. 1:4:0). We first identified aAPC-reactive $cytokine^+$ cells of both $CD4^+$ and $CD8^+$ T cells using the ORgate method, then downsampled these cells to 1000 per participant per condition, and subsequently utilized the Uniform Manifold Approximation and Projection (UMAP) algorithm[55] to visualize the various clusters of $CD4^+$ and $CD8^+$ T populations exerting effector functions. The identification of effector function clusters was performed using Phenograph.[56] As the goal of this analysis was to draw an effector function landscape rather than a phenotypic profiling, only cytokine parameters were loaded. The MFI from CD4 and CD8 markers were therefore not included in the UMAP calculation and did not contribute to the clustering. $CD4^+$ and $CD8^+$ cells could be identified *post-hoc* using categorical labels. Our approach generated 17 effector CD4 and CD8 T cell co-clusters (Figure 3A). The classification of clusters was based on distinct cytokine profiles indicated by fluorescent intensities (Figures 3B and S3A). Further qualification of the identified clusters was based on the percentage of cells expressing the different cytokines (Figure 3C).

This analysis revealed six clusters primarily composed of monofunctional cells (C4, C6, C8, C14, C15, C16), while the remaining clusters displayed varying degrees of polyfunctionality (Figure 3C). No cluster could be solely attributed to either the CD4 or the CD8 subset, or the presence or absence or CD28 co-stimulation. The most distinctive clusters between $CD4^+$ and $CD8^+$ T cells were C4, a mostly $CD4^+$ T cell cluster expressing only TNF, and C10, a mostly $CD8^+$ T cell cluster co-expressing IL-2 and IFNγ but not TNF. In $CD4^+$ T cells, IL-2 and IFNγ expression was frequent, and typically associated with TNF co-expression (Figures 3B–3E).

Although the main impact of CD28 co-stimulation was quantitative (Figures S3B and S3C), its relative influence varied among clusters, resulting in three distinct behaviors in $CD4^+$ T cells (Figure 3D): i) clusters whose relative importance declined with CD28 co-stimulation. These clusters (C1, C3, C4, C5, C6, C8, C11, C14) exhibited minimal or no IL-2 expression. These clusters were otherwise characterized by various degrees of TNFα, IFNγ or CD107a co-expression; ii) status quo, with clusters (C2, C7, C10, C15, C17) maintaining consistent proportions with or without CD28 co-stimulation. These clusters were characterized by a high degree of polyfunctionality, excepted for the cluster C15 that exerted only the IL-2 effector function; and iii) clusters enriched after co-stimulation with CD28. These clusters (C9, C12, C13, C16) expressed IL-2 and TNFα, or predominantly IL-2. CD28-mediated co-stimulation did not systematically increase polyfunctionality, as several polyfunctional clusters (C3, C5, C11) proportionally decreased in relative importance with CD28. Overall, similar observations were made on $CD8^+$ T cells, with minor cluster-specific differences (Figures 3E and S3C).

Principal component analyses (PCA) of T cell responses based on the proportions of these clusters in $CD4^+$ (Figure S3D) and $CD8^+$ (Figure S3E) T cells, illustrated the substantial effect of CD28 co-stimulation on the effector function profile. Therefore, CD28 serves a dual role by enhancing the potency of CD3-mediated TCR activation and fine-tuning the nature of the elicited effector functions.

CD28 co-stimulation enhances expression of second wave co-stimulatory molecules

In addition to CD28, a repertoire of other T cell co-stimulatory molecules exists, including CD69, CD40L, OX40, 4-1BB and ICOS. In contrast to the constitutive expression of CD28, these molecules typically undergo upregulation upon activation.[57–61] Our investigation aimed to assess the role of CD28 in their upregulation. T cells from uninfected control donors were stimulated with aAPCs for 15h, followed by surface marker staining and subsequent analysis by flow cytometry.

CD69 is a widely employed surface marker to monitor T cell activation due to its rapid and robust upregulation after T cell activation.[62,63] Notably, around one-third of $CD4^+$ T cells already expressed low levels of CD69 before stimulation (Figure 4A). This proportion increased to 73% upon exposure to aAPCs conjugated solely with aCD3, with further increase with the optimal 1:4 (aCD3:aCD28) aAPCs, reaching >95% of $CD4^+$ (Figure 4A) and $CD8^+$ (Figure S4A) T cells. To increase the accuracy of activated cell detection following aAPC stimulation, we analyzed CD69 in conjunction with other activation markers using an AND/OR Boolean strategy, an approach validated in previous studies.[64,65]

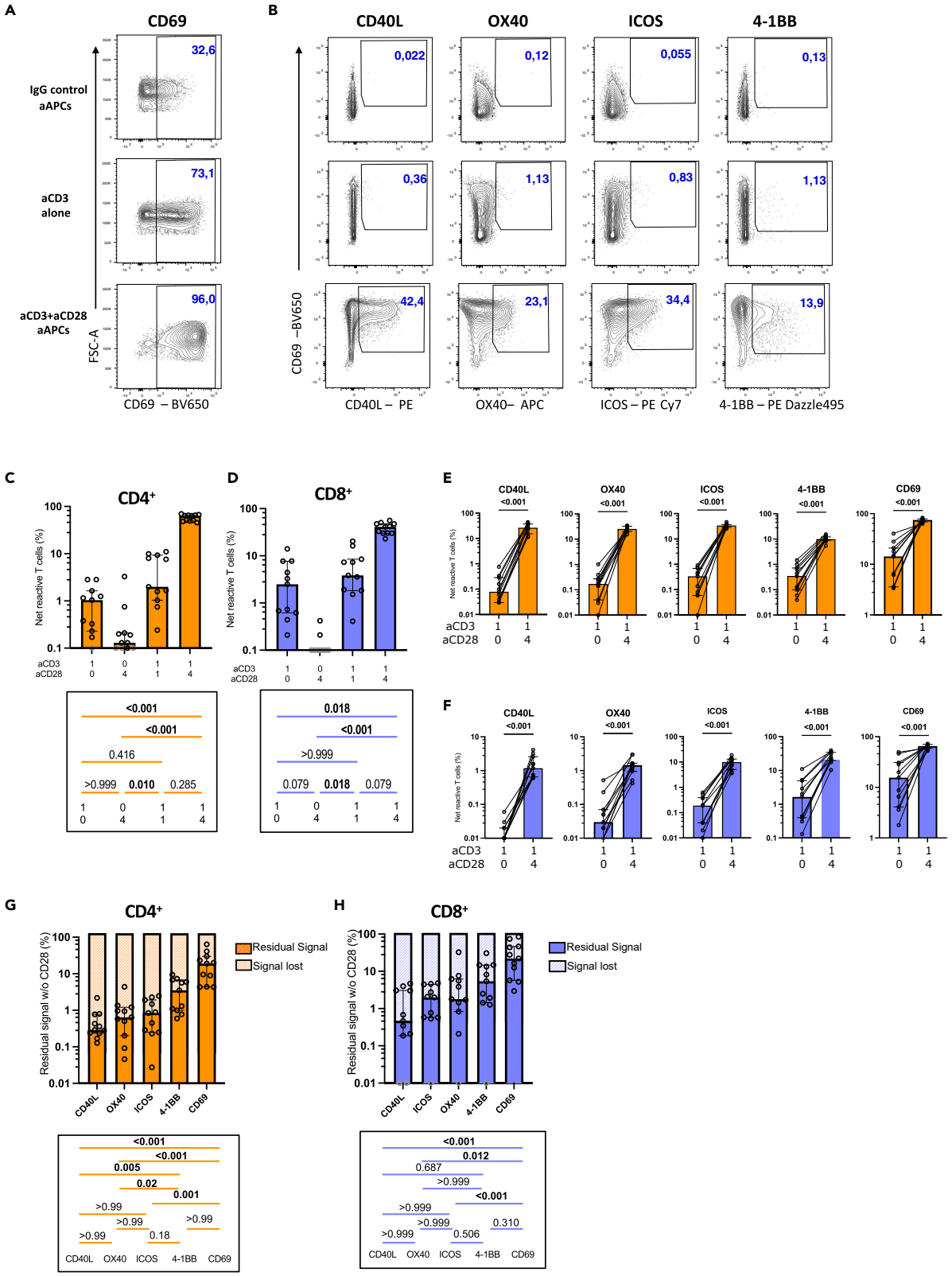
A
CD69
IgG control aAPCs
aCD3 alone
aCD3+aCD28 aAPCs
32,6
73,1
96,0
FSC-A
CD69 – BV650
B
CD40L
OX40
ICOS
4-1BB
0,022
0,12
0,055
0,13
0,36
1,13
0,83
1,13
42,4
23,1
34,4
13,9
CD69 –BV650
CD40L – PE
OX40– APC
ICOS – PE Cy7
4-1BB – PE Dazzle495
C
CD4+
Net reactive T cells (%)
aCD3
aCD28
<0.001
<0.001
0.416
>0.999
0.010
0.285
D
CD8+
0.018
<0.001
>0.999
0.079
0.018
0.079
E
CD40L
OX40
ICOS
4-1BB
CD69
<0.001
F
G
CD4+
Residual signal w/o CD28 (%)
Residual Signal
Signal lost
CD40L
OX40
ICOS
4-1BB
CD69
<0.001
0.005
0.02
0.001
>0.99
0.18
H
CD8+
0.012
0.687
0.310
0.506

Figure 4. CD28 co-stimulation enhances the expression of co-stimulatory molecules

Univariate analyses of co-stimulatory marker expression in $CD4^+$ and $CD8^+$ T cells after 15h of stimulation of purified T cells from UD participants, using aCD3 aAPCs or aCD3 aCD28 aAPCs.

(A and B) Representative flow cytometry plots of purified $CD4^+$ T cells stimulated with indicated aAPCs. (A) CD69 expression. (B) Co-expression of CD69 and other activation molecules.

(C–F) Background-subtracted net responses of $CD4^+$ and $CD8^+$ T cells expressing co-stimulation molecules (CD40L, OX40, 4-1BB, ICOS). Global responses (OR-gate identified cells expressing one or more co-stimulation molecules) for (C) $CD4^+$ and (D) $CD8^+$ T cells are shown, then subdivided individually for each tested co-stimulation molecule for (E) $CD4^+$ and (F) $CD8^+$.

(G and H) Percentage of residual $cytokine^+$ signal, representing the quotient between the 1:0:4 (aCD3:aCD28:IgG; aCD3 aAPCs) and 1:4:0 (aCD3:aCD28:IgG; aCD3+aCD28 aAPCs) conditions in (G) $CD4^+$ and (H) $CD8^+$ T cells. In (C–H), $n = 11$. Friedman tests are shown below the histograms in (C, D, G, H). In (C–H), error bars represent the interquartile range. Gray borders represent responses <0.1% (in C and D) or <0.01% (in H) that could not be represented on the logarithmic scale and hence were given arbitrary values of 0.1% or 0.01% respectively.

Consequently, co-expression of CD40L, OX40, 4-1BB, and ICOS with CD69 was quantified in $CD4^+$ and $CD8^+$ cells. Each activation marker was upregulated after aAPC stimulation, albeit to varying degrees (Figures 4B and S4B). Background signal was negligible (Figures S4C and S4D). We detected only minimal or no induction of T cell activation markers after stimulation with aAPCs incorporating solely aCD3 or aCD28 (Figures 4C–4F). Equimolar addition of CD28 (1:1 ratio of aCD3 to aCD28) marginally increased the signal (Figures 4C and 4D). In contrast, the proportion of activated cells sharply increased at the 1:4 (aCD3:aCD28) ratio, reaching a median of 62.6% in $CD4^+$ (Figure 4C) and 41.1% in $CD8^+$ (Figure 4D). This increase with co-stimulation was observed for all tested activation markers (Figures 4E and 4F).

As for the ICS assay, we calculated the residual signal in the absence of aCD28. In $CD4^+$ T cells, CD40L exhibited the highest dependency on CD28 co-stimulation followed by OX40, and ICOS. At the other end of the spectrum, 4-1BB and CD69 displayed greater independence from CD28 (Figure 4G). A comparable hierarchy was observed in $CD8^+$ T cells (Figure 4H). $CD8^+$ T cells exhibited less reliance on CD28 co-stimulation than in $CD4^+$ T cells across all markers except for CD40L, which was poorly expressed on $CD8^+$ T cells (Figure S4E). On a per-cell basis (median FI), CD28 co-stimulation increased the expression levels of CD40L, OX40, ICOS, and CD69, but not 4-1BB (Figures S4F and S4G).

In summary, these results reveal that activation markers have varying levels of dependency on CD28 co-stimulation, from stringent (OX40, CD40L, ICOS), to moderate (4-1BB), and low (CD69).

During viremic human immunodeficiency virus infection, the reliance on CD28 co-stimulation is heightened for IL-2, but diminished for interferon γ and TNFα

Inefficient CD28 co-stimulation has been reported during chronic viral infections.[26,66] Therefore, we sought to determine whether the dependence on CD28 co-stimulation was altered in the context of chronic HIV infection. We examined a cohort of 13 people with chronic HIV who had not yet initiated antiretroviral therapy (UNT) (Figure S5A); clinical characteristics are provided in Table S1.

Although not reaching significance, the stimulation with aCD3 aAPCs showed trends for higher levels of cytokine expression in both $CD4^+$ and $CD8^+$ T cells of UNT individuals compared to UD (Figures 5A, 5B, S5B, and S5C). Conversely, UNT's cytokine expression with CD28 co-stimulation showed trends for lower cytokine expression than those observed in UD (Figures S5B and S5C). We observed consistent results after correcting for the depletion of $CD4^+$ T cells, improving also the significance of the observation (Figures S5D and S5E). Consequently, these trends translated to a lower dependence for CD28 co-stimulation in UNT compared to UD people (Figures 5C and 5D). Notably, these findings were cytokine-dependent; while IFNγ and TNFα were significantly less reliant on CD28 co-stimulation in UNT donors, IL-2 demonstrated an opposing pattern, being more dependent on CD28 co-stimulation in UNT than in UD (Figures 5E and 5F).

We examined whether alterations in CD28 dependence were linked to changes in memory differentiation subsets (Figures S5F and S5G). In $CD4^+$ T cells from UNT, there were significantly lower frequencies of T_{TM} (Figures S5H). In $CD8^+$ T cells, T_{EM} and T_{EMRA} were elevated in UNT, whereas T_{CM} was concomitantly less frequent (Figures S5I). The increased dependence on CD28 co-stimulation for IL-2 in UNT was observed in all memory subsets. In contrast, the reduced dependence of IFNγ and TNFα on co-stimulation was specifically observed in the T_{EM} and T_{EMRA} subsets of UNT participants (Figures S5J and S5K).

These results reveal altered patterns of the requirement for CD28 co-stimulation in the context of chronic HIV infection, with cytokine-specific variations and memory subset influences.

$CD4^+$ and $CD8^+$ T cells from untreated people with human immunodeficiency virus exhibit effector functions skewed toward TNFα, interferon γ, and CD107a, and diminished IL-2 production

We employed an unsupervised approach to evaluate how the altered dependence on CD28 co-stimulation influenced the overall functional profile of $CD4^+$ and $CD8^+$ T cells during viremic HIV infection. $Cytokine^+$ $CD4^+$ and $CD8^+$ T cells from UNT, as defined in the ORgate analysis, were overlaid onto the UMAP analyses from Figure 3 (Figures 6A and 6B). We next compared the proportions of the aforementioned 17 identified clusters in UD and UNT participants. With regard to UNT vs. UD comparisons, these clusters displayed three distinct patterns (Figure 6C): i) clusters enriched in UNT compared to UD (C1, C2, C3, C4, C5, C6, C8. C11, C13. C14). These clusters expressed IFNγ, TNFα and/or CD107A, but not IL-2; ii) clusters similarly represented in both cohorts (C7, C16, C17); iii) clusters enriched in UD (C9, C10, C12, C15). These clusters were all characterized by IL-2 expression. $CD8^+$ T cell clusters exhibited more clusters enriched in UD, with additional $IL\text{-}2^+$ expressing clusters (C13, C16, C17) compared to $CD4^+$ T cells (Figure 6D). Notably, C5, characterized by IL17A expression, was similarly represented between cohorts

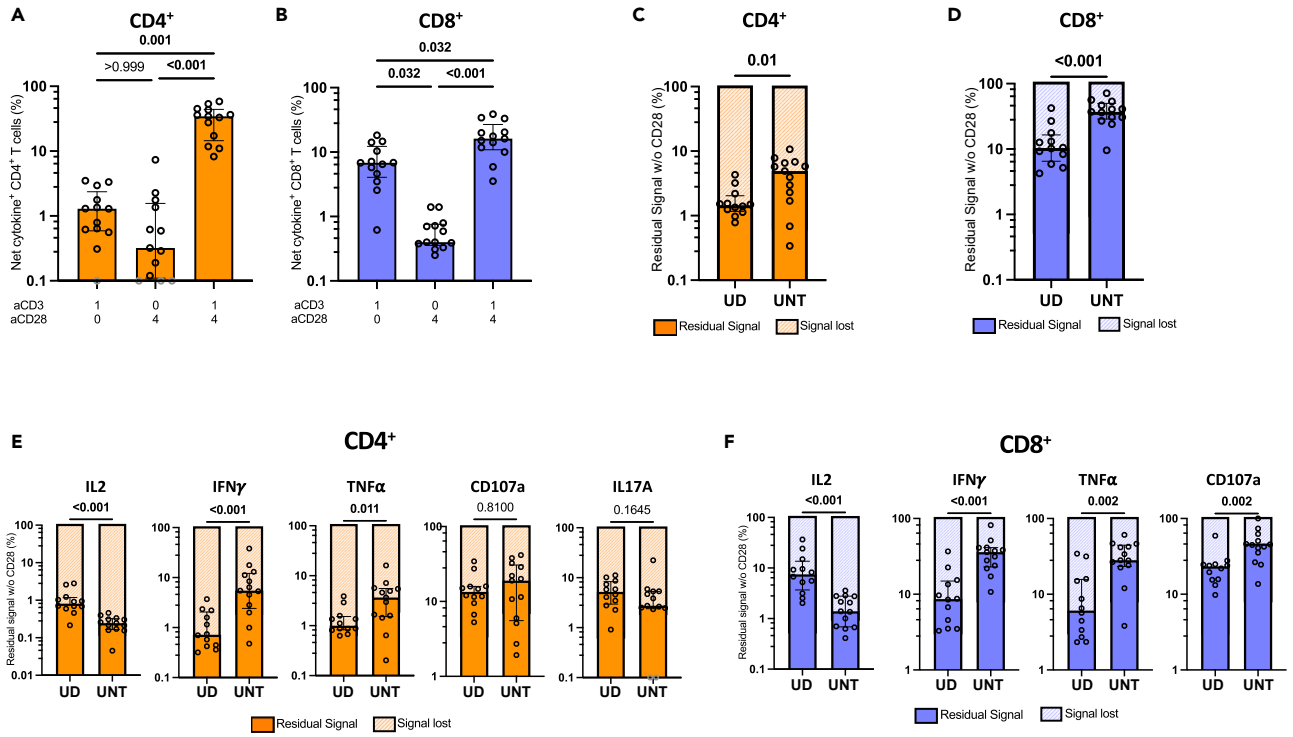

Figure 5. Cytokine-specific dependence on CD28 co-stimulation in untreated HIV infection

Univariate analyses of cytokine expression in CD4$^+$ and CD8$^+$ T cells after 15h of aAPCs stimulation of purified T cells from UD versus UNT participants. Unless specified, the ratios presented are 1:4:0 (aCD3:aCD28:IgG; aCD3 aCD28 aAPCs).

(A and B) ORgate-identified, background subtracted net (A) CD4$^+$ and (B) CD8$^+$ cytokine$^+$ T cell responses from UNT after aAPCs stimulation. Friedman test was used.

(C and D) Comparison of residual signal in the absence of CD28 co-stimulation for cytokine$^+$ (C) CD4$^+$ or (D) CD8$^+$ T cells in UD versus UNT participants.

(E and F) Comparison of residual signal in the absence of CD28 co-stimulation in (E) CD4$^+$ or (F) CD8$^+$ T cells between UD and UNT for each individual cytokine. In (C-F), Mann-Whitney test results are shown. In (A–F), $n = 12$. In (A-F), error bars represent the interquartile range. In (A) and (E), gray borders represent responses <0.1% that could not be represented on the logarithmic scale and hence were given arbitrary values of 0.1%.

in CD8$^+$ but higher in UNT's CD4$^+$ T cells. Globally, the clusters that are enriched in UNT compared to UD (C1, C2, C3, C4, C6, C8, C11, C14 for CD4 and CD8, and C5, C13 for CD4; C2 and C13 are the only exceptions) coincided with those that proportionally declined in the absence of CD28 co-stimulation. The overrepresentation of clusters less dependent on CD28 co-stimulation may thus represent a hallmark of the CD28 co-stimulation defect reported in UNT.

To further examine the alterations in functional profile during HIV infection, we integrated the proportions of CD4$^+$ and CD8$^+$ T cell clusters from UNT and UD controls in a principal component analysis (PCA) (Figures 6E and 6F). For both CD4$^+$ and CD8$^+$ T cells, we observed a clear and statistically significant separation of the two cohorts along the PC1 axis. To identify the cytokines driving this segregation, we correlated PC1 with the univariate percentage of each cytokine$^+$ T cell response (Figures 6G, 6H, S6A, and S6B). CD107a, IL17A, IFNγ, and TNFα all positively correlated with PC1 (or showed a trend in the case of TNFα in CD4$^+$), showing that the increased expression of these cytokines in UNT drove the observed separation (Figures 6G and 6H). Conversely, IL-2 correlated negatively with PC1, indicating that the diminished expression of this cytokine is a distinctive feature of UNT (Figures 6G and 6H). These findings were corroborated by univariate analyses, as we noted a lower proportion of IL-2$^+$ CD4$^+$ (Figure S6C) and CD8$^+$ (Figure S6D) T cells in UNT samples. Conversely, the proportion of IFNγ$^+$, TNFα$^+$ and CD107a$^+$ CD4$^+$ and CD8$^+$ T cells was higher in UNT than UD.

In summary, unsupervised integration of cytokine-positive T cell responses reveals distinct patterns enriched in UNT. Principal component analysis highlights the significant divergence between UNT and controls, driven by elevated IFNγ, TNFα, and CD107a alongside reduced IL-2 expression.

Initiation of antiretroviral treatment in people with human immunodeficiency virus partially normalizes cytokine profiles in CD4$^+$ T cells, with a limited impact on CD8$^+$ T cells

Next, we investigated whether ART could rectify the skewed functional profile observed during viremic HIV infection. We performed pairwise comparisons for participants with longitudinal follow-up and available pre- and post-ART leukapheresis samples (Table S1 and Figures S7A–S7C). The pairwise comparisons did not reveal statistically significant changes in global CD4$^+$ and CD8$^+$ cytokine T cell responses after ART,

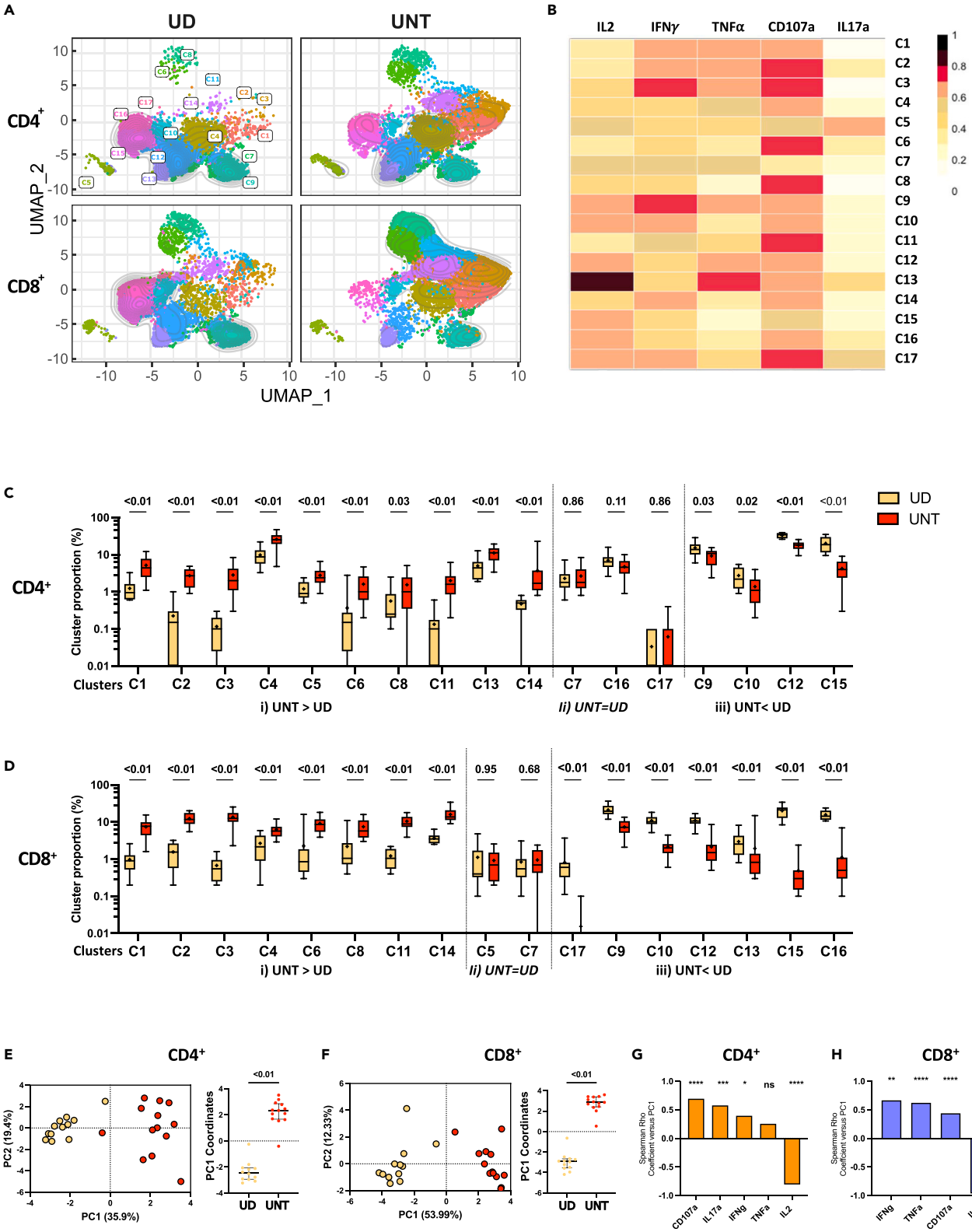
A
UD
UNT
CD4+
CD8+
UMAP_2
UMAP_1
B
IL2
IFNγ
TNFα
CD107a
IL17a
C1
C2
C3
C4
C5
C6
C7
C8
C9
C10
C11
C12
C13
C14
C15
C16
C17
C
CD4+
Cluster proportion (%)
Clusters
i) UNT > UD
ii) UNT=UD
iii) UNT< UD
D
CD8+
E
CD4+
PC2 (19.4%)
PC1 (35.9%)
PC1 Coordinates
F
CD8+
PC2 (12.33%)
PC1 (53.99%)
G
CD4+
Spearman Rho Coefficient versus PC1
CD107a
IL17a
IFNg
TNFa
IL2
H
CD8+
IFNg
TNFa
CD107a
IL2

Figure 6. Untreated PWH's CD4$^+$ and CD8$^+$ T cells show skewed effector functions

Multivariate analyses of cytokine expression in CD4$^+$ and CD8$^+$ T cells after 15h of aAPCs stimulation of purified T cells at the 1:4:0 (aCD3:aCD28:IgG; aCD3+aCD28 aAPCs) ratio. UD and UNT participants are herein qualitatively compared. Cytokine$^+$ CD4 and CD8 cells are identified by Boolean ORgate gating, downsampled to 1000 cell per participant per condition, concatenated, and then analyzed as follows.

(A) Multiparametric UMAP representation of cytokine$^+$ CD4$^+$ and CD8$^+$ T cells from UD or UNT, based on IL-2, IFNγ, TNFα, CD107a, and IL17A expression after stimulation with aAPCs (aCD3:aCD28:IgG 1:4:0). The colors identify the same 17 populations clustered by unsupervised analysis in Figure 3. The CD4$^+$ and CD8$^+$ categorical phenotypic information was reintroduced *post-hoc*.

(B) Heatmap summarizing the MFI of each parameter for each cluster (replicate of Figure 3B panel).

(C and D) Proportion of each cluster in the total, ORgate-defined cytokine+ population of (C) CD4$^+$ T cells and (D) CD8$^+$ T cells.

(E and F) Global PCA analysis (on the left) was done with the proportion cytokine$^+$ (E) CD4$^+$ or (F) CD8 $^+$ activated T cell clusters distinguishing UD (yellow) and UNT (red) participants. The percentage on the x and y axes represents the variance attributed to PC1 and PC2, respectively. On the right, histograms depicted the PC1 and PC2 values between the groups are shown.

(G and H) Spearman correlations between each individual cytokine and the PC1 values (*$p < 0.05$, **$p < 0.01$, ***$p < 0.001$) for (G) CD4 and (H) CD8. In (C–F), Mann-Whitney test results are shown. In (A–H), UD $n = 12$, UNT $n = 13$. In (C–F), error bars represent the interquartile range.

either with aCD3 alone or with CD28 co-stimulation (Figures 7A and 7B), beside slightly increased cytokine-positive CD4$^+$ T cell response to CD3 and CD28 co-stimulation in ART (Figures S7D and S7E). The residual cytokine response without CD28 was globally comparable before and after treatment (Figures 7C and 7D). This also held true for each individual cytokine assessed (Figures 7E and 7F).

Given that CD28 expression may influence dependence on co-stimulation, and that UNT have different memory subset compositions compared to UD (Figures S5F and S5G), we assessed CD28 expression in memory subsets from UNT and ART cohorts (Figures S7F–S7I). In CD4$^+$ T cells, almost 100% of TN, TCM, and TTM expressed CD28, but TEM and TEMRA had fewer CD28$^+$ cells in both UNT and ART cohorts. CD8$^+$ T cells showed similar tendencies, as more differentiated memory cells had a lower proportion of CD28$^+$ cells. However, the CD28 expression level per cell was similar between subsets, except for TN, which had slightly lower CD28 expression per CD28$^+$ cell.

We subsequently verified if the unsupervised analysis could reveal subtle qualitative differences between the effector profiles in UNT and ART (Figures 7G–7I). Following ART, some modest yet significant alterations were observed in the proportions of CD4$^+$ T cell clusters, with higher proportion of some IL-2$^+$ clusters (C12 and C15), and lower TNF$^+$ and CD107a$^+$ clusters (C2, C3, C4, C6, and C11) (Figure 7H). These combined alterations reflected a partial yet significant normalization of the CD4$^+$ T cell effector functions, as the ART group is located away from the UNT linearly along the PC1 axis toward the UD group on the PCA analysis plot (Figure 7J). After ART, IL-2$^+$ CD8 clusters were also increased (C12 and C15), and TNF$^+$ and CD107a$^+$ CD8 clusters decreased (C6, C8 and C11) (Figure 7I). These subtle alterations were sufficient to differentiate pre-ART and post-ART samples. However, this separation occurred along the PC2 axis, suggesting that these changes did not represent a normalization toward the UD group (Figure 7K).

These unsupervised analyses reveal that post-ART, global cytokine responses remain consistent, with treatment partially restoring CD4$^+$ T cell cytokine profiles, while CD8$^+$ T cell responses display limited changes.

DISCUSSION

In this study, we developed a versatile and convenient artificial Antigen-Presenting Cell (aAPC) system compatible with flow cytometry. It accommodates brief stimulation periods, fluid interfacing surfaces, and is tunable in terms of agonist antibody densities, as well as aAPC-to-cell ratios. This reductionist model enabled us to characterize in-depth the role of CD28 co-stimulation in primary CD4$^+$ and CD8$^+$ T cells isolated from blood samples, elucidating the varying levels of dependence of individual effector functions and secondary-wave activation molecules on this essential secondary signal. In control donors, our system highlights CD28's preferential enhancement of IL-2 expression and how this modulation shapes the elicited response profile, favoring it over other cytokines. Additionally, our analyses revealed that CD4$^+$ and CD8$^+$ T cells from viremic UNT prior to ART initiation exhibited a skewed orientation toward TNFα, IFNγ, and CD107a expression while diverging from IL-2 production. Expression of TNFα and IFNγ upon sole CD3 stimulation was relatively better preserved in viremic UNT compared to controls, in contrast to a more pronounced dependence on CD28 co-stimulation for IL-2 production. Importantly, this functional imbalance was only partially rectified by ART in CD4$^+$ but not in CD8$^+$ T cells.

Our artificial aAPC system induced robust T cell activation, with over 90% of CD4$^+$ and CD8$^+$ T cells expressing CD69 within just 15 h of stimulation, resulting in stronger activation than that achieved by directly cross-linking the antibodies. Furthermore, both T cell phenotype and viability were preserved following stimulation with aAPCs, unlike the results with magnetic CD3/CD28 beads, which in this experimental setup delivered a strong activation signal but at the cost of surface marker distortion, low cell yield, and high cell mortality.

The ratio of aCD3 to aCD28 antibodies embedded in aAPCs played a pivotal role in optimal cytokine expression. While the agonistic effect of aCD3 was fundamental, it reached a plateau swiftly in the absence of CD28 co-stimulation. In humans, inherited T cell CD28 deficiency leads to severe cutaneous lesions due to human papillomaviruses and moderate impairment of humoral responses, yet appear otherwise usually healthy.[67] This underscores the redundant nature of the co-stimulation process *in vivo*. For instance, murine studies in mice showed that CD27/CD70 signaling can substitute for CD28/B7 in LCMV-specific CD8$^+$ T cell expansion,[68] while another study showed that 4-1BBL could replace anti-CD28 as a co-stimulator.[69]

Our data indeed indicate that co-stimulation is necessary to optimally activate memory CD4$^+$ and CD8$^+$ T cells. This is consistent with murine studies that have demonstrated the essential role of CD28 in the recall responses of CD4$^+$ and CD8$^+$ T cells and subsequent viral clearance.[70,71] However, the extent of CD28 co-stimulation required depends on the differentiation state of the cell and was particularly important

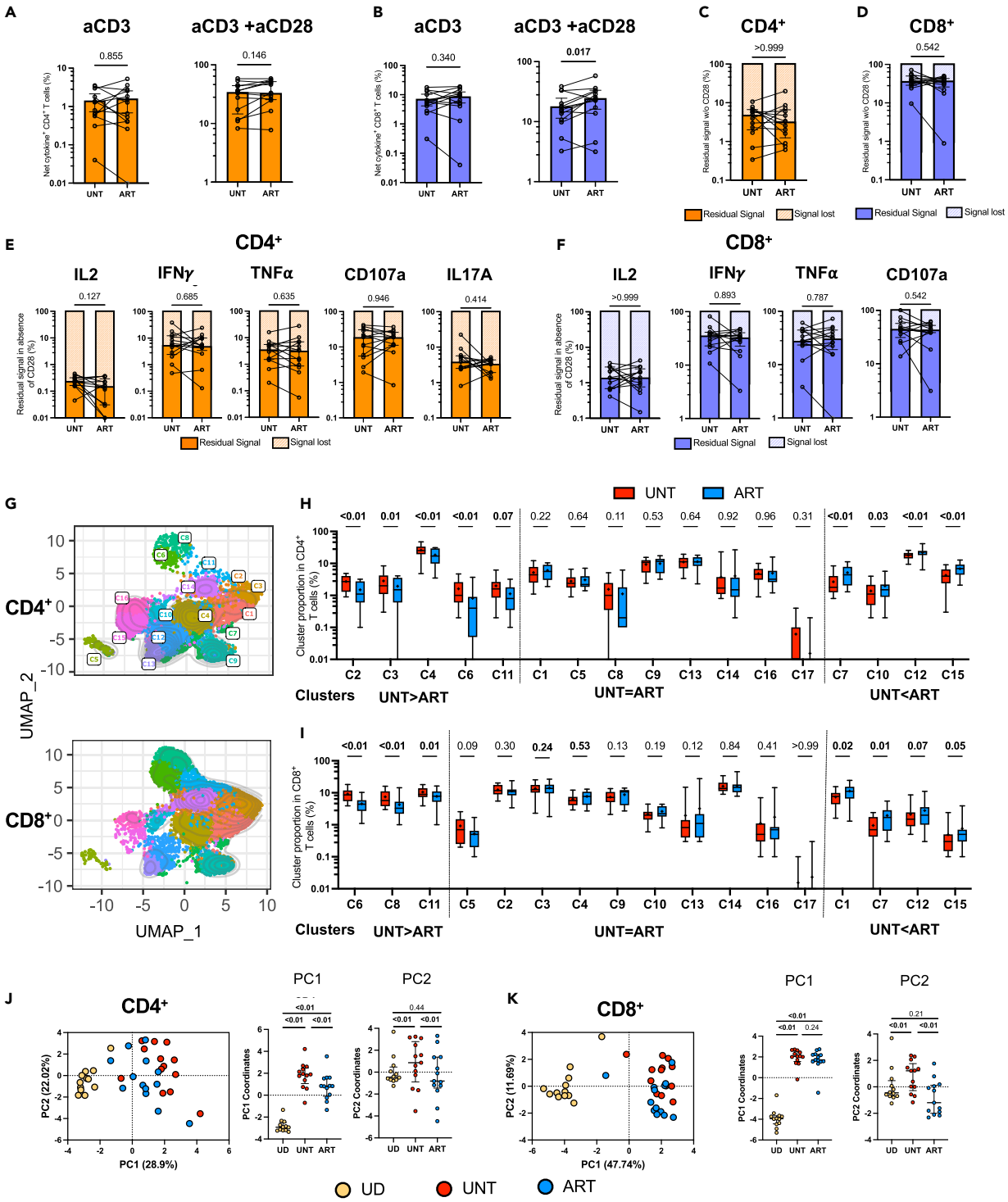

Figure 7. ART initiation in PWH partially normalizes cytokine profiles in CD4$^+$ T cells, with limited impact on CD8$^+$ T cells

(A–F) Univariate analyses of cytokine expression in CD4$^+$ and CD8$^+$ T cells after 15h of aAPCs stimulation of purified T cells from UNT versus ART participants.

(A and B) Comparison of total, ORgate-identified, background-subtracted, net cytokine+ (A) CD4$^+$ or (B) CD8$^+$ T cell responses in the UNT and ART cohorts after activation by aAPCs. Both 1:0:4 (aCD3:aCD28:IgG; aCD3 aAPCs, left panel) and 1:4:0 (aCD3:aCD28:IgG; aCD3+aCD28 aAPCs, right panel) stimulations are shown.

(C and D) Comparison of residual signal in the absence of CD28 co-stimulation of total cytokine$^+$ (C) CD4$^+$ or (D) CD8$^+$ T cells between UNT and ART.

(E and F) Comparison of residual signal in the absence of CD28 co-stimulation in CD4$^+$ (E) or CD8$^+$ (F) T cells between UNT and ART for each individual cytokine.

Figure 7. *Continued*

(G–K) Multivariate analyses of cytokine expression in $CD4^+$ and $CD8^+$ T cells after 15h of 1:4:0 (aCD3:aCD28:IgG; aCD3 aCD28 aAPCs) stimulation of purified T cells from UNT versus ART participants, following the same pipeline analyses as in Figures 3 and 6. The $CD4^+$ and $CD8^+$ categorical phenotypic information was reintroduced *post-hoc*. (G) Multiparametric UMAP representation of cytokine$^+$ $CD4^+$ and $CD8^+$ T cells from ART, based on IL-2, IFNγ, TNFα, CD107a, and IL17A expression after stimulation with aAPCs (aCD3:aCD28:IgG 1:4:0). The colors identify 17 populations clustered by unsupervised analysis using Phenograph. (H and I) Proportions of clusters among cytokine$^+$ (H) $CD4^+$ and (I) $CD8^+$ T cells in UNT vs. ART.

(J and K) Global PCA analysis (on the left) was done with the proportion of clusters in cytokine$^+$ (J) $CD4^+$ or (K) $CD8^+$ activated T cells. The percentage on the x and y axes presents the variance attributed to PC1 and PC2, respectively. On the right, plots of the PC1 and PC2 between groups are shown. In (A–K), UNT $n = 13$, ART $n = 13$. Wilcoxon test was used for paired comparisons between UNT and ART. In (A), gray borders represent responses <0.01% that could not be represented on the logarithmic scale and hence were given arbitrary values of 0.01%.

for naive and central memory cells. These less differentiated cells may require stronger co-activation signal to counter their relative quiescence, whereas effector memory and terminally differentiated cells are likely already poised for reactivation.

Co-stimulation is often understood as a mechanism for TCR signal amplification. Nevertheless, apart from globally increasing the expression of cytokines and activation markers, our data show that CD28 co-stimulation exerts a nuanced influence on the effector functions. Specifically, IL-2, IFNγ, TNFα, CD40L, OX40, and ICOS are preferentially promoted by CD28 compared to CD107a, IL17A, 4-1BB, and CD69. We observed that CD28 co-stimulation enriches certain T cell subpopulations that share IL-2 expression as a common feature. Indeed, CD28 is known to promote IL-2 expression by enhancing its transcription[72,73] and stabilizing its mRNA.[74] Additionally, CD28 has been found to induce DEC1, a transcription factor controlling IL-2 and IFNγ production.[75] Taken together with our findings, these studies suggest that CD28 co-stimulation can selectively promote the transcription of defined effector molecules. Alternatively, CD28 may more broadly impact cells committed to transcriptional programs that include certain functions, such as IL-2 and CD40L expression. The higher dependence on CD28 in the $CD4^+$ T cell lineage and in less differentiated cells is consistent with this interpretation. We cannot exclude that the dependence for CD28 co-stimulation can also be linked to the level of expression CD28. The lower dependence of TEMRA cells for CD28 co-stimulation coincides with their lower expression of surface CD28, which is consistent with this possibility (Figures S2K–S2M and S7F–S7M).[76,77] However, T_{EM} and T_{CM} expressed identical levels of CD28 yet were distinctly dependent on CD28 co-stimulation. Moreover, the different dependencies of the tested cytokines for CD28 suggest that other cellular features also play a role, such as the composition of the T cell population and possibly the expression of co-stimulatory and inhibitory receptors.

Compared to uninfected individuals, $CD4^+$ and $CD8^+$ T cells from UNT exhibited a greater overall responsiveness to the first signal given by aCD3, which could be attributed to the higher production of IFNγ and TNFα in response to aCD3. Conversely, we observed an increased dependency on CD28 for IL-2 in UNT. These altered dependencies on CD28 co-stimulation, seen in both naive and memory subsets, resulting in a distorted effector function profile characterized by increased frequencies of IFNγ and TNFα-expressing $CD4^+$ and $CD8^+$ T cell subsets, at the expense of IL-2-expressing subpopulations. The decreased IL-2 expression during HIV infection aligns with earlier reports on mitogen-stimulated PBMCs (such as phytohaemagglutinin PHA or PMA) from UNT.[78–81] Mitogen stimulation circumvents the TCR, which suggests that the altered effector profiles observed may stem from TCR-independent downstream signaling or mechanistic alterations that remain to be identified.

The precise molecular mechanisms underpinning the skewing of non-specific T cell effector functions during HIV infection remain incompletely understood. HIV variably affects $CD4^+$ T cell lineages and anatomic compartments, such as the preferential depletion of Th17 cells in the gut mucosa. This may lead to a preferential representation of other subsets in PWH.[82] Conversely, some populations are better restored during ART.[83,84] During HIV infection, the upregulation of immune checkpoints such as PD-1, CTLA-4, and Tim-3[23,85,86] is not restricted to HIV-specific responses but is broadly present in T cell subsets, which may contribute to dysfunction *in vivo*. Our engineered aAPCs bypass these pathways, as in contrast to natural APCs, they do not contain the corresponding ligands and interact with purified T cells. Therefore, while our data suggest T cell-intrinsic mechanisms, we cannot exclude the possibility that such signals triggered *in vivo* may have downstream effects in our assays. Consistent with this interpretation would be the epigenetic scars emerging from the persistent engagement of the PD1/PDL1 axis.[87,88] Other possible mechanisms include the persistent exposure to microbial products leaking from compromised intestinal barrier,[32] co-infection by cytomegalovirus (CMV) and Epstein-Barr virus (EBV),[89] and residual expression of HIV products,[90] which all contribute to a higher pro-inflammatory environment during ART. This may favor the expansion and maintenance of specific T cell subsets.[91]

Our data clarify the role of CD28 co-stimulation as a mechanism modulating both the magnitude and nature of effector functions triggered upon TCR-mediated activation in primary human blood cells. We observed distinct $CD4^+$ and $CD8^+$ T effector profiles during chronic HIV infection. Notably, these alterations were not specific to a specific pathogen. This skewing may undermine T cell responses against diverse antigens, thereby potentially contributing to HIV-associated co-morbidities.[92,93] Indeed, this non-specific skewing may introduce another layer of dysfunction whose impact, combined with HIV-specific $CD4^+$ and $CD8^+$ T cell impairment, could partially account for the well-documented residual immune dysfunction that persists despite ART (reviewed in[94]). Deciphering how these defects intertwine will be key to better understanding immune dysfunction during HIV infection.

Limitations of the study

Our experiments do not explore the contribution of other molecules that could compensate for suboptimal CD28 co-stimulation. Through the interaction of other agonistic antibodies or recombinant ligands, our aAPC system could be customized to specifically assess the involvement of other co-stimulatory or co-inhibitory molecules that modulate TCR signaling. This would necessitate the pre-emptive stimulation of T cells,

as most co-stimulatory molecules, apart from CD28, are not constitutively expressed on T cells but are expressed following a secondary wave of co-signaling molecules.[57–61]

Since many non-Th1 cytokine proteins are challenging to detect by flow cytometry, alternative readout approaches should be considered. Further studies should define alterations in the expression of other cytokines and chemokines not measured here, such as those preferentially produced by follicular helper T cells.[17] Some factors, such as age, sex, and co-morbidities, are known to influence the immune system,[95–97] but could not be investigated in this study due to the nature and size of the groups we examined.

The 1:4 (aCD3:aCD28) ratio was empirically determined. No ultrastructural studies were performed to verify the stochiometric implication of this ratio. It should not be interpretated as the necessity of 4 molecules of CD28 to ensure the co-stimulation of 1 molecule of CD3, as other factors such as antibody affinity can explained these empirically determined ratios.

Immune recovery during ART is variable, with a subpopulation of PWH presenting suboptimal CD4 T cell recovery, expansion of the CD8 compartment, and/or heightened inflammation despite optimal viral suppression. The aAPC system presented here could be used to compare immunological responders and non-responders in larger cohorts to identify features of persistent immune dysfunction on ART.

RESOURCE AVAILABILITY

Lead contact

For further information and requests related to resources and reagents, please contact Daniel E. Kaufmann at daniel.kaufmann@chuv.ch.

Materials availability

This study did not produce any new unique reagents.

Data and code availability

- The published article includes all datasets generated and analyzed for this study. For additional information and requests related to resources and reagents, please contact the lead contact Author (daniel.kaufmann@chuv.ch).
- All original code has been deposited at https://github.com/alemi055/scripts-and-data/blob/master/ShaabanKabakiboetal_2024.R and is publicly available as of the publication date. DOIs are listed in the key resources table.
- Any additional information required to reanalyze the data reported in this article is available from the lead contact upon request.

ACKNOWLEDGMENTS

The authors are grateful to the study participants. We thank Gaël Dulude, Philippe St-Onge, and the CRCHUM Flow Cytometry Platform; Olfa Debbeche and the CRCHUM BSL3 platform for technical assistance. We thank Olivier Tastet for his input on unsupervised analyses. This study was supported by the Canadian Institutes of Health Research (CIHR grant #168901 to D.E.K), the US National Institutes of Health (NIH grant HL092565 to D.E.K), an FRQS Merit Research Scholar Award (#268471 to D.E.K), and the Réseau Fonds de la recherche Québec-Santé (FRQ-S) SIDA & Maladies infectieuses and thérapies cellulaires. The Symphony flow cytometer was funded by a John R. Evans Leaders Fund from the Canada Foundation for Innovation (#37521 to D.E.K) and the Fondation Sclérodermie Québec. T.S.K and A.L. are supported by a scholarship from Canada Graduate Scholarships – Master's (CGS M) program, as well as the FRQS for A.L. T.S.K and E.A was supported by a PREMIER scholarship from Department of Medicine at University of Montreal. J.-P.R. is the holder of the Louis Lowenstein Chair at McGill University. The funders had no role in study design, data collection and analysis, decision to publish, or preparation of the article.

AUTHOR CONTRIBUTIONS

T.S.K, M.D., and D.E.K. designed the study; K.P. and E.A. optimized the aAPC system; G.O.D provided assistance with assay protocols; T.S.K. and E.A. performed the experiments; T.S. and A.L. analyzed the data; A.L performed the unsupervised analysis; T.S.K., M.D., N.S. and D.E.K. interpreted the data; T.S.K., M.D., and D.E.K. wrote the initial draft of the article; all co-authors reviewed and edited the article; proofreading was accomplished by M.D., T.S.K., and D.E.K. AI-assisted software was used to help with proofreading. N.S., M.D., and D.E.K. provided supervision.

DECLARATION OF INTERESTS

The authors declare no competing interests.

DECLARATION OF GENERATIVE AI AND AI-ASSISTED TECHNOLOGIES IN THE WRITING PROCESS

During the preparation of this work, and after having written a complete version of the text, the authors used GPT 4 from OpenAI and Grammarly in order to improve language and readability, as they are not native English speakers. After using this tool, the authors reviewed and edited the content as needed and take full responsibility for the content of the publication.

STAR★METHODS

Detailed methods are provided in the online version of this paper and include the following:

- Crosslinking antibodies
- CD3/CD28 Dynabeads
- Intracellular cytokine staining (ICS)
- Activation-induced marker (AIM) assay
- Unsupervised clustering

- QUANTIFICATION AND STATISTICAL ANALYSIS
  - Statistical analyses

SUPPLEMENTAL INFORMATION

Supplemental information can be found online at https://doi.org/10.1016/j.isci.2024.110947.

Received: October 13, 2023
Revised: February 16, 2024
Accepted: September 10, 2024
Published: September 13, 2024

REFERENCES

1. Bretscher, P., and Cohn, M. (1970). A theory of self-nonself discrimination. Science *169*, 1042–1049. https://doi.org/10.1126/science.169.3950.1042.
2. Garcia, K.C., Degano, M., Pease, L.R., Huang, M., Peterson, P.A., Teyton, L., and Wilson, I.A. (1998). Structural basis of plasticity in T cell receptor recognition of a self peptide-MHC antigen. Science *279*, 1166–1172. https://doi.org/10.1126/science.279.5354.1166.
3. Coyle, A.J., and Gutierrez-Ramos, J.C. (2001). The expanding B7 superfamily: increasing complexity in costimulatory signals regulating T cell function. Nat. Immunol. *2*, 203–209. https://doi.org/10.1038/85251.
4. Linterman, M.A., Denton, A.E., Divekar, D.P., Zvetkova, I., Kane, L., Ferreira, C., Veldhoen, M., Clare, S., Dougan, G., Espéli, M., and Smith, K.G.C. (2014). CD28 expression is required after T cell priming for helper T cell responses and protective immunity to infection. Elife *3*, e03180. https://doi.org/10.7554/eLife.03180.
5. Rodríguez-Palmero, M., Hara, T., Thumbs, A., and Hünig, T. (1999). Triggering of T cell proliferation through CD28 induces GATA-3 and promotes T helper type 2 differentiation *in vitro* and *in vivo*. Eur. J. Immunol. *29*, 3914–3924. https://doi.org/10.1002/(sici)1521-4141(199912)29:12<3914::Aid-immu3914>3.0.Co;2-#.
6. Frauwirth, K.A., Riley, J.L., Harris, M.H., Parry, R.V., Rathmell, J.C., Plas, D.R., Elstrom, R.L., June, C.H., and Thompson, C.B. (2002). The CD28 signaling pathway regulates glucose metabolism. Immunity *16*, 769–777. https://doi.org/10.1016/s1074-7613(02)00323-0.
7. Martin, P.J., Ledbetter, J.A., Morishita, Y., June, C.H., Beatty, P.G., and Hansen, J.A. (1986). A 44 kilodalton cell surface homodimer regulates interleukin 2 production by activated human T lymphocytes. J. Immunol. *136*, 3282–3287.
8. Boise, L.H., Minn, A.J., Noel, P.J., June, C.H., Accavitti, M.A., Lindsten, T., and Thompson, C.B. (1995). CD28 costimulation can promote T cell survival by enhancing the expression of Bcl-XL. Immunity *3*, 87–98. https://doi.org/10.1016/1074-7613(95)90161-2.
9. Thomas, R.M., Gao, L., and Wells, A.D. (2005). Signals from CD28 induce stable epigenetic modification of the IL-2 promoter. J. Immunol. *174*, 4639–4646. https://doi.org/10.4049/jimmunol.174.8.4639.
10. Butte, M.J., Lee, S.J., Jesneck, J., Keir, M.E., Haining, W.N., and Sharpe, A.H. (2012). CD28 costimulation regulates genome-wide effects on alternative splicing. PLoS One *7*, e40032. https://doi.org/10.1371/journal.pone.0040032.
11. DuPage, M., Chopra, G., Quiros, J., Rosenthal, W.L., Morar, M.M., Holohan, D., Zhang, R., Turka, L., Marson, A., and Bluestone, J.A. (2015). The chromatin-modifying enzyme Ezh2 is critical for the maintenance of regulatory T cell identity after activation. Immunity *42*, 227–238. https://doi.org/10.1016/j.immuni.2015.01.007.
12. Wada, N.I., Jacobson, L.P., Margolick, J.B., Breen, E.C., Macatangay, B., Penugonda, S., Martínez-Maza, O., and Bream, J.H. (2015). The effect of HAART-induced HIV suppression on circulating markers of inflammation and immune activation. AIDS *29*, 463–471. https://doi.org/10.1097/qad.0000000000000545.
13. French, M.A., King, M.S., Tschampa, J.M., da Silva, B.A., and Landay, A.L. (2009). Serum immune activation markers are persistently increased in patients with HIV infection after 6 years of antiretroviral therapy despite suppression of viral replication and reconstitution of CD4+ T cells. J. Infect. Dis. *200*, 1212–1215. https://doi.org/10.1086/605890.
14. Lindqvist, M., van Lunzen, J., Soghoian, D.Z., Kuhl, B.D., Ranasinghe, S., Kranias, G., Flanders, M.D., Cutler, S., Yudanin, N., Muller, M.I., et al. (2012). Expansion of HIV-specific T follicular helper cells in chronic HIV infection. J. Clin. Invest. *122*, 3271–3280. https://doi.org/10.1172/jci64314.
15. Champagne, P., Ogg, G.S., King, A.S., Knabenhans, C., Ellefsen, K., Nobile, M., Appay, V., Rizzardi, G.P., Fleury, S., Lipp, M., et al. (2001). Skewed maturation of memory HIV-specific CD8 T lymphocytes. Nature *410*, 106–111. https://doi.org/10.1038/35065118.
16. Niessl, J., Baxter, A.E., Morou, A., Brunet-Ratnasingham, E., Sannier, G., Gendron-Lepage, G., Richard, J., Delgado, G.G., Brassard, N., Turcotte, I., et al. (2020). Persistent expansion and Th1-like skewing of HIV-specific circulating T follicular helper cells during antiretroviral therapy. EBioMedicine *54*, 102727. https://doi.org/10.1016/j.ebiom.2020.102727.
17. Morou, A., Brunet-Ratnasingham, E., Dubé, M., Charlebois, R., Mercier, E., Darko, S., Brassard, N., Nganou-Makamdop, K., Arumugam, S., Gendron-Lepage, G., et al. (2019). Altered differentiation is central to HIV-specific CD4(+) T cell dysfunction in progressive disease. Nat. Immunol. *20*, 1059–1070. https://doi.org/10.1038/s41590-019-0418-x.
18. Goepfert, P.A., Bansal, A., Edwards, B.H., Ritter, G.D., Jr., Tellez, I., McPherson, S.A., Sabbaj, S., and Mulligan, M.J. (2000). A significant number of human immunodeficiency virus epitope-specific cytotoxic T lymphocytes detected by tetramer binding do not produce gamma interferon. J. Virol. *74*, 10249–10255. https://doi.org/10.1128/jvi.74.21.10249-10255.2000.
19. Kostense, S., Vandenberghe, K., Joling, J., Van Baarle, D., Nanlohy, N., Manting, E., and Miedema, F. (2002). Persistent numbers of tetramer+ CD8(+) T cells, but loss of interferon-gamma+ HIV-specific T cells during progression to AIDS. Blood *99*, 2505–2511. https://doi.org/10.1182/blood.v99.7.2505.
20. Shankar, P., Russo, M., Harnisch, B., Patterson, M., Skolnik, P., and Lieberman, J. (2000). Impaired function of circulating HIV-specific CD8(+) T cells in chronic human immunodeficiency virus infection. Blood *96*, 3094–3101.
21. Appay, V., Nixon, D.F., Donahoe, S.M., Gillespie, G.M., Dong, T., King, A., Ogg, G.S., Spiegel, H.M., Conlon, C., Spina, C.A., et al. (2000). HIV-specific CD8(+) T cells produce antiviral cytokines but are impaired in cytolytic function. J. Exp. Med. *192*, 63–75. https://doi.org/10.1084/jem.192.1.63.
22. Lichterfeld, M., Kaufmann, D.E., Yu, X.G., Mui, S.K., Addo, M.M., Johnston, M.N., Cohen, D., Robbins, G.K., Pae, E., Alter, G., et al. (2004). Loss of HIV-1-specific CD8+ T cell proliferation after acute HIV-1 infection and restoration by vaccine-induced HIV-1-specific CD4+ T cells. J. Exp. Med. *200*, 701–712. https://doi.org/10.1084/jem.20041270.
23. Day, C.L., Kaufmann, D.E., Kiepiela, P., Brown, J.A., Moodley, E.S., Reddy, S., Mackey, E.W., Miller, J.D., Leslie, A.J., DePierres, C., et al. (2006). PD-1 expression on HIV-specific T cells is associated with

T-cell exhaustion and disease progression. Nature *443*, 350–354. https://doi.org/10.1038/nature05115.

24. Barber, D.L., Wherry, E.J., Masopust, D., Zhu, B., Allison, J.P., Sharpe, A.H., Freeman, G.J., and Ahmed, R. (2006). Restoring function in exhausted CD8 T cells during chronic viral infection. Nature *439*, 682–687. https://doi.org/10.1038/nature04444.
25. Wherry, E.J., Ha, S.J., Kaech, S.M., Haining, W.N., Sarkar, S., Kalia, V., Subramaniam, S., Blattman, J.N., Barber, D.L., and Ahmed, R. (2007). Molecular signature of CD8+ T cell exhaustion during chronic viral infection. Immunity *27*, 670–684. https://doi.org/10.1016/j.immuni.2007.09.006.
26. Hui, E., Cheung, J., Zhu, J., Su, X., Taylor, M.J., Wallweber, H.A., Sasmal, D.K., Huang, J., Kim, J.M., Mellman, I., and Vale, R.D. (2017). T cell costimulatory receptor CD28 is a primary target for PD-1-mediated inhibition. Science *355*, 1428–1433. https://doi.org/10.1126/science.aaf1292.
27. Hazenberg, M.D., Stuart, J.W., Otto, S.A., Borleffs, J.C., Boucher, C.A., de Boer, R.J., Miedema, F., and Hamann, D. (2000). T-cell division in human immunodeficiency virus (HIV)-1 infection is mainly due to immune activation: a longitudinal analysis in patients before and during highly active antiretroviral therapy (HAART). Blood *95*, 249–255.
28. Doisne, J.M., Urrutia, A., Lacabaratz-Porret, C., Goujard, C., Meyer, L., Chaix, M.L., Sinet, M., and Venet, A. (2004). CD8+ T cells specific for EBV, cytomegalovirus, and influenza virus are activated during primary HIV infection. J. Immunol. *173*, 2410–2418. https://doi.org/10.4049/jimmunol.173.4.2410.
29. Copeland, N.K., Eller, M.A., Kim, D., Creegan, M., Esber, A., Eller, L.A., Semwogerere, M., Kibuuka, H., Kiweewa, F., Crowell, T.A., et al. (2021). Brief Report: Increased Inflammation and Liver Disease in HIV/HBV-Coinfected Individuals. J. Acquir. Immune Defic. Syndr. *88*, 310–313. https://doi.org/10.1097/qai.0000000000002760.
30. Righetti, E., Ballon, G., Ometto, L., Cattelan, A.M., Menin, C., Zanchetta, M., Chieco-Bianchi, L., and De Rossi, A. (2002). Dynamics of Epstein-Barr virus in HIV-1-infected subjects on highly active antiretroviral therapy. AIDS *16*, 63–73. https://doi.org/10.1097/00002030-200201040-00009.
31. Jabs, D.A., Enger, C., and Bartlett, J.G. (1989). Cytomegalovirus retinitis and acquired immunodeficiency syndrome. Arch. Ophthalmol. *107*, 75–80. https://doi.org/10.1001/archopht.1989.01070010077031.
32. Brenchley, J.M., Price, D.A., Schacker, T.W., Asher, T.E., Silvestri, G., Rao, S., Kazzaz, Z., Bornstein, E., Lambotte, O., Altmann, D., et al. (2006). Microbial translocation is a cause of systemic immune activation in chronic HIV infection. Nat. Med. *12*, 1365–1371. https://doi.org/10.1038/nm1511.
33. Younas, M., Psomas, C., Reynes, C., Cezar, R., Kundura, L., Portales, P., Merle, C., Atoui, N., Fernandez, C., Le Moing, V., et al. (2019). Microbial Translocation Is Linked to a Specific Immune Activation Profile in HIV-1-Infected Adults With Suppressed Viremia. Front. Immunol. *10*, 2185. https://doi.org/10.3389/fimmu.2019.02185.
34. Bürgisser, P., Hammann, C., Kaufmann, D., Battegay, M., and Rutschmann, O.T. (1999). Expression of CD28 and CD38 by CD8+ T lymphocytes in HIV-1 infection correlates with markers of disease severity and changes towards normalization under treatment. The Swiss HIV Cohort Study. Clin. Exp. Immunol. *115*, 458–463. https://doi.org/10.1046/j.1365-2249.1999.00818.x.
35. Kaizuka, Y., Douglass, A.D., Varma, R., Dustin, M.L., and Vale, R.D. (2007). Mechanisms for segregating T cell receptor and adhesion molecules during immunological synapse formation in Jurkat T cells. Proc. Natl. Acad. Sci. USA *104*, 20296–20301. https://doi.org/10.1073/pnas.0710258105.
36. Grakoui, A., Bromley, S.K., Sumen, C., Davis, M.M., Shaw, A.S., Allen, P.M., and Dustin, M.L. (1999). The immunological synapse: a molecular machine controlling T cell activation. Science *285*, 221–227. https://doi.org/10.1126/science.285.5425.221.
37. Ilani, T., Vasiliver-Shamis, G., Vardhana, S., Bretscher, A., and Dustin, M.L. (2009). T cell antigen receptor signaling and immunological synapse stability require myosin IIA. Nat. Immunol. *10*, 531–539. https://doi.org/10.1038/ni.1723.
38. Yokosuka, T., Kobayashi, W., Sakata-Sogawa, K., Takamatsu, M., Hashimoto-Tane, A., Dustin, M.L., Tokunaga, M., and Saito, T. (2008). Spatiotemporal regulation of T cell costimulation by TCR-CD28 microclusters and protein kinase C theta translocation. Immunity *29*, 589–601. https://doi.org/10.1016/j.immuni.2008.08.011.
39. Bromley, S.K., Iaboni, A., Davis, S.J., Whitty, A., Green, J.M., Shaw, A.S., Weiss, A., and Dustin, M.L. (2001). The immunological synapse and CD28-CD80 interactions. Nat. Immunol. *2*, 1159–1166. https://doi.org/10.1038/ni737.
40. Dustin, M.L. (2010). Insights into function of the immunological synapse from studies with supported planar bilayers. Curr. Top. Microbiol. Immunol. *340*, 1–24. https://doi.org/10.1007/978-3-642-03858-7_1.
41. Mescher, M.F. (1992). Surface contact requirements for activation of cytotoxic T lymphocytes. J. Immunol. *149*, 2402–2405.
42. Perica, K., Tu, A., Richter, A., Bieler, J.G., Edidin, M., and Schneck, J.P. (2014). Magnetic field-induced T cell receptor clustering by nanoparticles enhances T cell activation and stimulates antitumor activity. ACS Nano *8*, 2252–2260. https://doi.org/10.1021/nn405520d.
43. Hsu, C.J., Hsieh, W.T., Waldman, A., Clarke, F., Huseby, E.S., Burkhardt, J.K., and Baumgart, T. (2012). Ligand mobility modulates immunological synapse formation and T cell activation. PLoS One *7*, e32398. https://doi.org/10.1371/journal.pone.0032398.
44. Giannoni, F., Barnett, J., Bi, K., Samodal, R., Lanza, P., Marchese, P., Billetta, R., Vita, R., Klein, M.R., Prakken, B., et al. (2005). Clustering of T cell ligands on artificial APC membranes influences T cell activation and protein kinase C theta translocation to the T cell plasma membrane. J. Immunol. *174*, 3204–3211. https://doi.org/10.4049/jimmunol.174.6.3204.
45. Olden, B.R., Perez, C.R., Wilson, A.L., Cardle, I.I., Lin, Y.S., Kaehr, B., Gustafson, J.A., Jensen, M.C., and Pun, S.H. (2019). Cell-Templated Silica Microparticles with Supported Lipid Bilayers as Artificial Antigen-Presenting Cells for T Cell Activation. Adv. Healthcare Mater. *8*, e1801188. https://doi.org/10.1002/adhm.201801188.
46. Chen, J.Y., Agrawal, S., Yi, H.P., Vallejo, D., Agrawal, A., and Lee, A.P. (2023). Cell-Sized Lipid Vesicles as Artificial Antigen-Presenting Cells for Antigen-Specific T Cell Activation. Adv. Healthcare Mater. *12*, e2203163. https://doi.org/10.1002/adhm.202203163.
47. Goldstein, S.A., and Mescher, M.F. (1986). Cell-sized, supported artificial membranes (pseudocytes): response of precursor cytotoxic T lymphocytes to class I MHC proteins. J. Immunol. *137*, 3383–3392.
48. Cheung, A.S., Zhang, D.K.Y., Koshy, S.T., and Mooney, D.J. (2018). Scaffolds that mimic antigen-presenting cells enable ex vivo expansion of primary T cells. Nat. Biotechnol. *36*, 160–169. https://doi.org/10.1038/nbt.4047.
49. Kim, H.S., Ho, T.C., Willner, M.J., Becker, M.W., Kim, H.W., and Leong, K.W. (2023). Dendritic cell-mimicking scaffolds for ex vivo T cell expansion. Bioact. Mater. *21*, 241–252. https://doi.org/10.1016/j.bioactmat.2022.08.015.
50. Wauters, A.C., Scheerstra, J.F., Vermeijlen, I.G., Hammink, R., Schluck, M., Woythe, L., Wu, H., Albertazzi, L., Figdor, C.G., Tel, J., et al. (2022). Artificial Antigen-Presenting Cell Topology Dictates T Cell Activation. ACS Nano *16*, 15072–15085. https://doi.org/10.1021/acsnano.2c06211.
51. Zhang, D.K.Y., Cheung, A.S., and Mooney, D.J. (2020). Activation and expansion of human T cells using artificial antigen-presenting cell scaffolds. Nat. Protoc. *15*, 773–798. https://doi.org/10.1038/s41596-019-0249-0.
52. Lemieux, A., Sannier, G., Nicolas, A., Nayrac, M., Delgado, G.G., Cloutier, R., Brassard, N., Laporte, M., Duchesne, M., Sreng Flores, A.M., et al. (2024). Enhanced detection of antigen-specific T cells by a multiplexed AIM assay. Cell Rep. Methods *4*, 100690. https://doi.org/10.1016/j.crmeth.2023.100690.
53. de Araújo-Souza, P.S., Hanschke, S.C.H., Nardy, A.F.F.R., Sécca, C., Oliveira-Vieira, B., Silva, K.L., Soares-Lima, S.C., and Viola, J.P.B. (2020). Differential interferon-γ production by naive and memory-like CD8 T cells. J. Leukoc. Biol. *108*, 1329–1337. https://doi.org/10.1002/jlb.2ab0420-646r.
54. Sallusto, F., Lenig, D., Förster, R., Lipp, M., and Lanzavecchia, A. (1999). Two subsets of memory T lymphocytes with distinct homing potentials and effector functions. Nature *401*, 708–712. https://doi.org/10.1038/44385.
55. Becht, E., McInnes, L., Healy, J., Dutertre, C.A., Kwok, I.W.H., Ng, L.G., Ginhoux, F., and Newell, E.W. (2018). Dimensionality reduction for visualizing single-cell data using UMAP. Nat. Biotechnol. *37*, 38–44. https://doi.org/10.1038/nbt.4314.
56. Levine, J.H., Simonds, E.F., Bendall, S.C., Davis, K.L., Amir, E.a.D., Tadmor, M.D., Litvin, O., Fienberg, H.G., Jager, A., Zunder, E.R., et al. (2015). Data-Driven Phenotypic Dissection of AML Reveals Progenitor-like Cells that Correlate with Prognosis. Cell *162*, 184–197. https://doi.org/10.1016/j.cell.2015.05.047.
57. Noelle, R.J., Roy, M., Shepherd, D.M., Stamenkovic, I., Ledbetter, J.A., and Aruffo, A. (1992). A 39-kDa protein on activated helper T cells binds CD40 and transduces

the signal for cognate activation of B cells. Proc. Natl. Acad. Sci. USA *89*, 6550–6554. https://doi.org/10.1073/pnas.89.14.6550.

58. Kinnear, G., Wood, K.J., Fallah-Arani, F., and Jones, N.D. (2013). A diametric role for OX40 in the response of effector/memory CD4+ T cells and regulatory T cells to alloantigen. J. Immunol. *191*, 1465–1475. https://doi.org/10.4049/jimmunol.1300553.
59. Gramaglia, I., Weinberg, A.D., Lemon, M., and Croft, M. (1998). Ox-40 ligand: a potent costimulatory molecule for sustaining primary CD4 T cell responses. J. Immunol. *161*, 6510–6517.
60. Pollok, K.E., Kim, Y.J., Zhou, Z., Hurtado, J., Kim, K.K., Pickard, R.T., and Kwon, B.S. (1993). Inducible T cell antigen 4-1BB. Analysis of expression and function. J. Immunol. *150*, 771–781.
61. Hutloff, A., Dittrich, A.M., Beier, K.C., Eljaschewitsch, B., Kraft, R., Anagnostopoulos, I., and Kroczek, R.A. (1999). ICOS is an inducible T-cell co-stimulator structurally and functionally related to CD28. Nature *397*, 263–266. https://doi.org/10.1038/16717.
62. Maino, V.C., Suni, M.A., and Ruitenberg, J.J. (1995). Rapid flow cytometric method for measuring lymphocyte subset activation. Cytometry *20*, 127–133. https://doi.org/10.1002/cyto.990200205.
63. Simms, P.E., and Ellis, T.M. (1996). Utility of flow cytometric detection of CD69 expression as a rapid method for determining poly- and oligoclonal lymphocyte activation. Clin. Diagn. Lab. Immunol. *3*, 301–304. https://doi.org/10.1128/cdli.3.3.301-304.1996.
64. Reiss, S., Baxter, A.E., Cirelli, K.M., Dan, J.M., Morou, A., Daigneault, A., Brassard, N., Silvestri, G., Routy, J.P., Havenar-Daughton, C., et al. (2017). Comparative analysis of activation induced marker (AIM) assays for sensitive identification of antigen-specific CD4 T cells. PLoS One *12*, e0186998. https://doi.org/10.1371/journal.pone.0186998.
65. Porichis, F., Hart, M.G., Zupkosky, J., Barblu, L., Kwon, D.S., McMullen, A., Brennan, T., Ahmed, R., Freeman, G.J., Kavanagh, D.G., and Kaufmann, D.E. (2014). Differential impact of PD-1 and/or interleukin-10 blockade on HIV-1-specific CD4 T cell and antigen-presenting cell functions. J. Virol. *88*, 2508–2518. https://doi.org/10.1128/jvi.02034-13.
66. Kamphorst, A.O., Wieland, A., Nasti, T., Yang, S., Zhang, R., Barber, D.L., Konieczny, B.T., Daugherty, C.Z., Koenig, L., Yu, K., et al. (2017). Rescue of exhausted CD8 T cells by PD-1-targeted therapies is CD28-dependent. Science *355*, 1423–1427. https://doi.org/10.1126/science.aaf0683.
67. Béziat, V., Rapaport, F., Hu, J., Titeux, M., Bonnet des Claustres, M., Bourgey, M., Griffin, H., Bandet, É., Ma, C.S., Sherkat, R., et al. (2021). Humans with inherited T cell CD28 deficiency are susceptible to skin papillomaviruses but are otherwise healthy. Cell *184*, 3812–3828.e30. https://doi.org/10.1016/j.cell.2021.06.004.
68. Welten, S.P.M., Redeker, A., Franken, K.L.M.C., Oduro, J.D., Ossendorp, F., Čičin-Šain, L., Melief, C.J.M., Aichele, P., and Arens, R. (2015). The viral context instructs the redundancy of costimulatory pathways in driving CD8(+) T cell expansion. Elife *4*, e07486. https://doi.org/10.7554/eLife.07486.
69. Saoulli, K., Lee, S.Y., Cannons, J.L., Yeh, W.C., Santana, A., Goldstein, M.D., Bangia, N., DeBenedette, M.A., Mak, T.W., Choi, Y., and Watts, T.H. (1998). CD28-independent, TRAF2-dependent costimulation of resting T cells by 4-1BB ligand. J. Exp. Med. *187*, 1849–1862. https://doi.org/10.1084/jem.187.11.1849.
70. Borowski, A.B., Boesteanu, A.C., Mueller, Y.M., Carafides, C., Topham, D.J., Altman, J.D., Jennings, S.R., and Katsikis, P.D. (2007). Memory CD8+ T cells require CD28 costimulation. J. Immunol. *179*, 6494–6503. https://doi.org/10.4049/jimmunol.179.10.6494.
71. Ndejembi, M.P., Teijaro, J.R., Patke, D.S., Bingaman, A.W., Chandok, M.R., Azimzadeh, A., Nadler, S.G., and Farber, D.L. (2006). Control of memory CD4 T cell recall by the CD28/B7 costimulatory pathway. J. Immunol. *177*, 7698–7706. https://doi.org/10.4049/jimmunol.177.11.7698.
72. Fraser, J.D., Irving, B.A., Crabtree, G.R., and Weiss, A. (1991). Regulation of interleukin-2 gene enhancer activity by the T cell accessory molecule CD28. Science *251*, 313–316. https://doi.org/10.1126/science.1846244.
73. Verweij, C.L., Geerts, M., and Aarden, L.A. (1991). Activation of interleukin-2 gene transcription via the T-cell surface molecule CD28 is mediated through an NF-kB-like response element. J. Biol. Chem. *266*, 14179–14182.
74. Lindstein, T., June, C.H., Ledbetter, J.A., Stella, G., and Thompson, C.B. (1989). Regulation of lymphokine messenger RNA stability by a surface-mediated T cell activation pathway. Science *244*, 339–343. https://doi.org/10.1126/science.2540528.
75. Martínez-Llordella, M., Esensten, J.H., Bailey-Bucktrout, S.L., Lipsky, R.H., Marini, A., Chen, J., Mughal, M., Mattson, M.P., Taub, D.D., and Bluestone, J.A. (2013). CD28-inducible transcription factor DEC1 is required for efficient autoreactive CD4+ T cell response. J. Exp. Med. *210*, 1603–1619. https://doi.org/10.1084/jem.20122387.
76. Salumets, A., Tserel, L., Rumm, A.P., Türk, L., Kingo, K., Saks, K., Oras, A., Uibo, R., Tamm, R., Peterson, H., et al. (2022). Epigenetic quantification of immunosenescent CD8(+) TEMRA cells in human blood. Aging Cell *21*, e13607. https://doi.org/10.1111/acel.13607.
77. Koch, S., Larbi, A., Derhovanessian, E., Ozcelik, D., Naumova, E., and Pawelec, G. (2008). Multiparameter flow cytometric analysis of CD4 and CD8 T cell subsets in young and old people. Immun. Ageing *5*, 1–12. https://doi.org/10.1186/1742-4933-5-6.
78. Clerici, M., Hakim, F.T., Venzon, D.J., Blatt, S., Hendrix, C.W., Wynn, T.A., and Shearer, G.M. (1993). Changes in interleukin-2 and interleukin-4 production in asymptomatic, human immunodeficiency virus-seropositive individuals. J. Clin. Invest. *91*, 759–765. https://doi.org/10.1172/jci116294.
79. Westby, M., Marriott, J.B., Guckian, M., Cookson, S., Hay, P., and Dalgleish, A.G. (1998). Abnormal intracellular IL-2 and interferon-gamma (IFN-gamma) production as HIV-1-assocated markers of immune dysfunction. Clin. Exp. Immunol. *111*, 257–263. https://doi.org/10.1046/j.1365-2249.1998.00505.x.
80. Clerici, M., and Shearer, G.M. (1993). A TH1–>TH2 switch is a critical step in the etiology of HIV infection. Immunol. Today *14*, 107–111. https://doi.org/10.1016/0167-5699(93)90208-3.
81. Klein, S.A., Dobmeyer, J.M., Dobmeyer, T.S., Pape, M., Ottmann, O.G., Helm, E.B., Hoelzer, D., and Rossol, R. (1997). Demonstration of the Th1 to Th2 cytokine shift during the course of HIV-1 infection using cytoplasmic cytokine detection on single cell level by flow cytometry. AIDS *11*, 1111–1118. https://doi.org/10.1097/00002030-199709000-00005.
82. Le Hingrat, Q., Sereti, I., Landay, A.L., Pandrea, I., and Apetrei, C. (2021). The Hitchhiker Guide to CD4(+) T-Cell Depletion in Lentiviral Infection. A Critical Review of the Dynamics of the CD4(+) T Cells in SIV and HIV Infection. Front. Immunol. *12*, 695674. https://doi.org/10.3389/fimmu.2021.695674.
83. Lu, L., Li, X., Liu, X., Qiu, Z., Han, Y., Song, X., Li, Y., Li, X., Cao, W., Lv, W., et al. (2022). The pattern and magnitude of T cell subsets reconstitution during ten years of ART with viral suppression in HIV-infected patients. Aging (Albany NY) *14*, 9647–9667. https://doi.org/10.18632/aging.204416.
84. Renault, C., Veyrenche, N., Mennechet, F., Bedin, A.S., Routy, J.P., Van de Perre, P., Reynes, J., and Tuaillon, E. (2022). Th17 CD4+ T-Cell as a Preferential Target for HIV Reservoirs. Front. Immunol. *13*, 822576. https://doi.org/10.3389/fimmu.2022.822576.
85. Kaufmann, D.E., Kavanagh, D.G., Pereyra, F., Zaunders, J.J., Mackey, E.W., Miura, T., Palmer, S., Brockman, M., Rathod, A., Piechocka-Trocha, A., et al. (2007). Upregulation of CTLA-4 by HIV-specific CD4+ T cells correlates with disease progression and defines a reversible immune dysfunction. Nat. Immunol. *8*, 1246–1254. https://doi.org/10.1038/ni1515.
86. Jones, R.B., Ndhlovu, L.C., Barbour, J.D., Sheth, P.M., Jha, A.R., Long, B.R., Wong, J.C., Satkunarajah, M., Schweneker, M., Chapman, J.M., et al. (2008). Tim-3 expression defines a novel population of dysfunctional T cells with highly elevated frequencies in progressive HIV-1 infection. J. Exp. Med. *205*, 2763–2779. https://doi.org/10.1084/jem.20081398.
87. Youngblood, B., Noto, A., Porichis, F., Akondy, R.S., Ndhlovu, Z.M., Austin, J.W., Bordi, R., Procopio, F.A., Miura, T., Allen, T.M., et al. (2013). Cutting edge: Prolonged exposure to HIV reinforces a poised epigenetic program for PD-1 expression in virus-specific CD8 T cells. J. Immunol. *191*, 540–544. https://doi.org/10.4049/jimmunol.1203161.
88. Ahn, E., Youngblood, B., Lee, J., Lee, J., Sarkar, S., and Ahmed, R. (2016). Demethylation of the PD-1 Promoter Is Imprinted during the Effector Phase of CD8 T Cell Exhaustion. J. Virol. *90*, 8934–8946. https://doi.org/10.1128/jvi.00798-16.
89. Gianella, S., Moser, C., Vitomirov, A., McKhann, A., Layman, L., Scott, B., Caballero, G., Lada, S., Bosch, R.J., Hoenigl, M., et al. (2020). Presence of asymptomatic cytomegalovirus and Epstein–Barr virus DNA in blood of persons with HIV starting antiretroviral therapy is associated with non-AIDS clinical events. AIDS *34*, 849–857. https://doi.org/10.1097/qad.0000000000002484.

90. Sannier, G., Dubé, M., Dufour, C., Richard, C., Brassard, N., Delgado, G.G., Pagliuzza, A., Baxter, A.E., Niessl, J., Brunet-Ratnasingham, E., et al. (2021). Combined single-cell transcriptional, translational, and genomic profiling reveals HIV-1 reservoir diversity. Cell Rep. *36*, 109643. https://doi.org/10.1016/j.celrep.2021.109643.

91. Osuji, F.N., Onyenekwe, C.C., Ahaneku, J.E., and Ukibe, N.R. (2018). The effects of highly active antiretroviral therapy on the serum levels of pro-inflammatory and anti-inflammatory cytokines in HIV infected subjects. J. Biomed. Sci. *25*, 88. https://doi.org/10.1186/s12929-018-0490-9.

92. Babu, H., Ambikan, A.T., Gabriel, E.E., Svensson Akusjärvi, S., Palaniappan, A.N., Sundaraj, V., Mupanni, N.R., Sperk, M., Cheedarla, N., Sridhar, R., et al. (2019). Systemic Inflammation and the Increased Risk of Inflamm-Aging and Age-Associated Diseases in People Living With HIV on Long Term Suppressive Antiretroviral Therapy. Front. Immunol. *10*, 1965. https://doi.org/10.3389/fimmu.2019.01965.

93. Lederman, M.M., Funderburg, N.T., Sekaly, R.P., Klatt, N.R., and Hunt, P.W. (2013). Residual immune dysregulation syndrome in treated HIV infection. Adv. Immunol. *119*, 51–83. https://doi.org/10.1016/b978-0-12-407707-2.00002-3.

94. Cai, C.W., and Sereti, I. (2021). Residual immune dysfunction under antiretroviral therapy. Semin. Immunol. *51*, 101471. https://doi.org/10.1016/j.smim.2021.101471.

95. Teissier, T., Boulanger, E., and Cox, L.S. (2022). Interconnections between Inflammageing and Immunosenescence during Ageing. Cells *11*, 359. https://doi.org/10.3390/cells11030359.

96. Klein, S.L., and Flanagan, K.L. (2016). Sex differences in immune responses. Nat. Rev. Immunol. *16*, 626–638. https://doi.org/10.1038/nri.2016.90.

97. Poon, M.M.L., Byington, E., Meng, W., Kubota, M., Matsumoto, R., Grifoni, A., Weiskopf, D., Dogra, P., Lam, N., Szabo, P.A., et al. (2021). Heterogeneity of human anti-viral immunity shaped by virus, tissue, age, and sex. Cell Rep. *37*, 110071. https://doi.org/10.1016/j.celrep.2021.110071.

98. Sannier, G., Nicolas, A., Dubé, M., Marchitto, L., Nayrac, M., Tastet, O., Chatterjee, D., Tauzin, A., Lima-Barbosa, R., Laporte, M., et al. (2023). A third SARS-CoV-2 mRNA vaccine dose in people receiving hemodialysis overcomes B cell defects but elicits a skewed CD4(+) T cell profile. Cell Rep Med *4*, 100955. https://doi.org/10.1016/j.xcrm.2023.100955.

99. Hahne, F., LeMeur, N., Brinkman, R.R., Ellis, B., Haaland, P., Sarkar, D., Spidlen, J., Strain, E., and Gentleman, R. (2009). flowCore: a Bioconductor package for high throughput flow cytometry. BMC Bioinf. *10*, 106. https://doi.org/10.1186/1471-2105-10-106.

100. Quintelier, K., Couckuyt, A., Emmaneel, A., Aerts, J., Saeys, Y., and Van Gassen, S. (2021). Analyzing high-dimensional cytometry data using FlowSOM. Nat. Protoc. *16*, 3775–3801. https://doi.org/10.1038/s41596-021-00550-0.

101. Nayrac, M., Dubé, M., Sannier, G., Nicolas, A., Marchitto, L., Tastet, O., Tauzin, A., Brassard, N., Lima-Barbosa, R., Beaudoin-Bussières, G., et al. (2022). Temporal associations of B and T cell immunity with robust vaccine responsiveness in a 16-week interval BNT162b2 regimen. Cell Rep. *39*, 111013. https://doi.org/10.1016/j.celrep.2022.111013.

102. John, C.R., Watson, D., Russ, D., Goldmann, K., Ehrenstein, M., Pitzalis, C., Lewis, M., and Barnes, M. (2020). M3C: Monte Carlo reference-based consensus clustering. Sci. Rep. *10*, 1816. https://doi.org/10.1038/s41598-020-58766-1.

103. Wickham, H. (2016). ggplot2 Elegant Graphics for Data Analysis (Springer Cham). https://doi.org/10.1007/978-3-319-24277-4.

104. Kolde, R. (2019). Pheatmap: Pretty Heatmaps.

STAR★METHODS

KEY RESOURCES TABLE

REAGENT or RESOURCE	SOURCE	IDENTIFIER
Antibodies		
UCHT1 (BUV395) [Human anti-CD3]	BD Bioscience	Cat#563546; Lot: 1214287; RRID:AB_2744387
SK3 (BUV496) [Human anti-CD4]	BD Bioscience	Cat#612936; Lot: 2140305; RRID:AB_2870220
HI100 (BUV563) [Human anti-CD45RA]	BD Bioscience	Cat#612926; Lot: 1078217; RRID:AB_2870211
L128 (BUV661) [Human anti-CD27]	BD Bioscience	Ca#750167; Lot: 3021264; RRID:AB_2874372
NK-1 (BV421) [Human anti-CD57]	Biolegend	Cat#393326; Lot: B361783 ; RRID:AB_2860964
M5E2 (BV480) [Human anti-CD14]	BD Bioscience	Cat#746304; Lot 2286909; RRID:AB_2743629
HIB19 (BV480) [Human anti-CD19]	BD Bioscience	Cat#746457; Lot: 2286911; RRID:AB_2743759
RPA-T8 (BV570) [Human anti-CD8]	Biolegend	Cat#301038; Lot: B346256; RRID:AB_2563213
H4A3 (BV786) [Humananti-CD107a]	BD Bioscience	Cat#563869; Lot: 1207206; RRID:AB_2738458
Mab11 (AF488) [Human anti-TNFα]	Biolegend	Cat#502915; Lot: B311742; RRID:AB_493121
FN50 (PerCPeF710) [Human anti-CD69]	ebioscience	Cat#46-0699-42; Lot: 2514279; RRID:AB_2573694
REA1063 (PE) [Human anti- IL17a]	Miltenyi	Cat#130-118-243; Lot: 1323010976; RRID:AB_2751466
MQ1-17H12 (PE-Dazzle594) [Human anti-IL-2]	Biolegend	Cat#500344; Lot:B351592; RRID:AB_2564091
(PE-Cy7) [Human anti-IFNγ]	BD Bioscience	Cat#557643; Lot: 1229911; RRID:AB_396760
2-L1-A (APC-R700) [Human anti-CCR7]	BD Bioscience	Cat#566766; Lot: 2257402; RRID:AB_2869856
TRAP1 (APC) [Human anti-CD40L]	BD Bioscience	Cat#555702; Lot: 2010706; RRID:AB_398610
LIVE/DEAD Fixable dead cell	BD Bioscience	Cat#L34960 ;Lot:2433781
CD28.2 (BUV737) [Human anti-CD28]	BD Bioscience	Cat#612815; Lot: 2251073; RRID:AB_2870140
EH12.2 (BB515) [Human anti-PD-1]	BD Bioscience	Cat#564494; Lot: 2101875; RRID:AB_2738827
FN50 (BV650) [Human anti-CD69]	Biolegend	Cat#310934; Lot:B360356; RRID:AB_2563158
MBSA43 (PerCPeF710) [Human anti-TIGIT]	Invitrogen ebioscience	Cat#46-9500-42; Lot:2402674; RRID:AB_10853679
4B4-1 (PE-Dazzle594) [Human anti-4-1BB]	Biolegend	Cat#309826; Lot:B349385; RRID:AB_2566259
ISA-3 (PE-Cy7) [Human anti-ICOS]	Invitrogen ebioscience	Cat#25-9948-42; Lot: 2338678; RRID:AB_1518754
ACT35 (APC) [Human anti-OX40]	BD Bioscience	Cat# 563473; Lot: 2026053; RRID:AB_2738230
TRAP (PE) [Human anti-CD40L]	BD Bioscience	Cat#555700; Lot: 0357889; RRID:AB_396050
CD3 Antibody, anti-human, Biotin functional grade	Miltenyi	Cat#130-093-377; Lot: 5210202091; RRID:AB_1036126
Biotin anti-human CD28	Biolegend	Cat:302904; Lot: B394472; RRID:AB_314306
Biotin Mouse IgG1, κ Isotype Ctrl Antibody	Biolegend	Cat#400104; Lot: B350305; RRID:AB_326427
Purified Goat anti-mouse IgG (minimal x-reactivity) Antibody	Biolegend	Cat# 405301; Lot: B343022 RRID:AB_315005
Chemicals, peptides, and recombinant proteins		
Staphylococcal Enterotoxin B (SEB)	Toxin technology	Cat#BT202
Silica microspheres	Bangs Laboratoreis	Cat# SS05003 ; Lot: 16497
Srteptavidin	Jackson ImmunoResearch	Cat#016-000-084; Lot: 154826
18:1 (Δ9-Cis) PC (DOPC)	Avanti polar (via sigma)	Cat# 850375C-200mg
18:1 DGS-NTA(Ni)	Avanti polar (via sigma)	Cat# 790404C-10mg
18:1 Biotinyl Cap PE	Avanti polar (via sigma)	Cat#870273C-25mg
RPMI 1640	GIBCO by Life Technologies	Cat# 11875-119

(*Continued on next page*)

Continued

REAGENT or RESOURCE	SOURCE	IDENTIFIER
HEPES	Invitrogen	Cat# 15630-080
Penicillin-Streptomycin	GIBCO by Life Technologies	Cat# 15140-122
Nuclease S7 from Staphylococcus aureus	Roche Diagnostics	Cat# 12344000
Bovine Serum Albumin	Sigma-Aldrich	Cat#A2153-50G CAS#9048-46-8
BD GolgiStop (Monensin)	BD Bioscience	Cat# 554724
BD GolgiPlug (Brefeldin A)	BD Bioscience	Cat#555029
FcR Blocking Reagent, human	Miltenyi	Cat#130-059-901
Invitrogen™ UltraPure™ Tris Buffer (powder format)	Invitrogen	Cat#15504020
Critical commercial assays		
EasySep Human T Cell Enrichment Kit	StemCell	Cat# 19051_C
Dynabeads Human T-Activator CD3/CD28 - for physiological activation of human T cells	ThermoFisher	Cat# 11161D; Lot:2860963; RRID:AB_2916088
Deposited data		
Original code is deposited at	N/A	"Original Code : https://github.com/alemi055/scripts-and-data/blob/master/ShaabanKabakiboetal_2024.R"
Software and algorithms		
Flow Jo v10.8.0	Flow Jo	https://www.flowjo.com
GraphPad Prism v8.4.1	GraphPad	https://www.graphpad.com

EXPERIMENTAL MODEL AND STUDY PARTICIPANT DETAILS

Ethics statement

All work was conducted in accordance with the Declaration of Helsinki regarding informed consent and approval by an appropriate institutional board. Leukaphereses were obtained from study participants at the Montreal General Hospital, Montreal, Canada and at the Centre Hospitalier de l'Université de Montréal (CHUM) in Montreal, Canada. The study was approved by the respective Institutional Review Boards (IRB CHUM: 17.335) and participants gave written informed consent prior to enrollment. Samples were collected between 2013 and 2019 as part of a multicentric study (MP-37-2018-4029).

Study participants

Subject characteristics are summarized in Table S1. Uninfected donors (UD) are free of HIV-1 infection. Untreated HIV participants had plasma viral loads of at least 5000 copies/ml (except for one at 2700 copies/mL), had been documented by blood testing to live with HIV for at least three months, and were either untreated or off ART for at least 3 months at the time of collection of the "Pre-ART" sample. Longitudinal "Post-ART" samples were collected in these same subjects after at least 6 months on ART and achieving controlled viremia (<50 vRNA copies/mL). PBMCs were isolated from blood samples by Ficoll density gradient centrifugation and cryopreserved in liquid nitrogen until use.

METHOD DETAILS

Liposomes preparation

DOPC, Cap biotin PE and Ni-NTA DOGS lipids were purchased from Avanti Polar Lipids at stock concentrations of 25 mg/mL (DOPC) or 10 mg/mL (biotin-PE and Ni-NTA DOGS) in chloroform layered in argon and stored at -20°C upon receipt (Cat #850375C, #870273C, and #790404C respectively). All lipid solutions were always stored under argon to avoid oxidation. Chloroform solutions of lipids were mixed to obtain a final 4 mM DOPC solution after hydration with DOPC (98%), Cap biotin PE (2%) and Ni-NTA (6.25%) (molar ratios). Lipids were first dried under nitrogen stream and left to completely dry for 2h. The dry lipid film was rehydrated in nitrogen-purged Tris-saline for 30 min at room temperature until the solution became homogenous. The unilamellar liposomes were passed 10 times through a polycarbonate membrane (0.1 μm) in an extruder (Avanti Polar Lipids, Cat #610000) to produce bilayered liposomes (LUVs). The liposome solution was then diluted 10 times to obtain the working stock solution.

Artificial APCs preparation

aAPCs were freshly prepared on the day of stimulation. All centrifuging was done at 600g for 2 min at room temperature. Lipid bilayered aAPCs were obtained by washing 5-μm silica beads (Bangs laboratories, Cat #SS06N) twice with water, then vigorous vortexing with liposome

bilayer suspension (2 μL of 1X liposomes solution per 1 μL (1M/μL) of beads) during four sequences of 10 seconds each. Ligands addition and quantities were adapted to experiment requirements and cells number required for flow cytometry each time. Briefly, the lipid-coated beads were washed once with filtered HBS-BSA buffer and incubated with 4 μg/mL streptavidin (Jackson Immunoresearch, Cat #016-000-084) for 30 min at room temperature, then washed again with HBS-BSA buffer. Streptavidin coated beads were incubated 30 min at room temperature with anti-CD3-biotin (0.585 μg/mL) and anti-CD28-biotin (2.344 μg/mL) in HBS-BSA 1% buffer for a aCD3:aCD28 ratio 1:4. Concentrations of aCD3 and aCD28 were adapted for different ratios, and the corresponding Isotype IgG concentration was complemented on suboptimal aAPCs to reach an overall antibody concentration equivalent to that of the aCD3:CD28 1:4 ratio condition. Beads were finally washed with HBS-BSA buffer and resuspended in the proper amount of HBS-BSA.

PBMCs thawing, purification, and stimulation

Frozen PBMCs were thawed in Fetal Bovine Serum (FBS) before total T cells isolation by negative magnetic bead selection (EasySep™ Human T Cell Isolation Kit). Purified T cells were resuspended at 8×10^6/mL in RPMI (GIBCO by Life Technologies) supplemented with penicillin/streptomycin (GIBCO by Life Technologies) and 10% of FBS, and rested for 2 hours. Two million purified T cells were stimulated with aAPCs at a cell:bead ratio of 1:4. As a positive control, 2 million PBMCs were stimulated by 0.5 μL of 1 μg/mL SEB. PBMCs were used for SEB activation instead of purified T cells because SEB activity requires MHC on natural antigen-presenting cells.

Crosslinking antibodies

After resting, two million T cells [8 million/mL] were either left unstimulated or incubated with anti-CD3-biotin (1.5 ug/mL) and anti-CD28-biotin (6 ug/mL) antibodies on ice for 15 minutes, followed by washig with the same culture media. Surface-bound antibodies were subsequently cross-linked using various concentrations of purified goat anti-mouse IgG (Poly4053). Cells were then incubated for 15 hours at 37°C.

CD3/CD28 Dynabeads

Dynabeads were first washed with phosphate buffered saline (PBS 1X) and resuspended in culture media at their original concentration ($4x10^7$ beads/mL). After resting, two million T cells [8 million/mL] were either left unstimulated or incubated with Dynabeads at a cell-to-beads ratio of 1:1 for 15h at 37°C. Before flow cytometric analysis, Dynabeads were removed using a magnet.

Intracellular cytokine staining (ICS)

Cell stimulation was carried out for 15h in the presence of mouse anti-human CD107a and anti-human CCR7 at 37°C and 5% CO2. Brefeldin A and monensin (BD Biosciences, San Jose, CA) were added 1h after stimulation. Following stimulation, cells were washed by PBS 1X, and stained for a viability dye (Aquavivid, Thermo Fisher scientific, Waltham, MA) for 20 min at room temperature in PBS. Cells were then stained for surface markers (CD3, CD4, CD45RA, CD27, CD57, CD8, CD19, CD14) for 30 min at 4°C. This was followed by intracellular detection of cytokines (IL-2, IFNγ, TNFα, CD107a, IL17A) using the IC Fixation/Permeabilization kit (Thermo Fisher scientific, Waltham, MA), according to the manufacturer's protocol. Cells were acquired on a Symphony flow cytometer (BD Biosciences) and analyzed using FlowJo v10.8.1 software. Antibodies used are listed in Table S2. To calculate the degree of dependence on CD28, we used this formula : $Residual\ signal\ without\ CD28 = \frac{cytokine^+\ cells\ activated\ by\ CD3\ alone(aCD3{:}aCD28{:}IgG\ 1{:}0{:}4)}{cytokine^+\ cells\ activated\ by\ CD3{+}CD28(aCD3{:}aCD28{:}IgG\ 1{:}4{:}0)}$.

To correct for CD4 counts in UNT and ART in each participant, we used this formula : $Net\ cytokine^+ cells/mm^3 = [\%\ cytokine^+ cells] \times [CD4\ cells\ count\ /mm^3]$.

Activation-induced marker (AIM) assay

The AIM assay was performed as previously reported.[98] Cells were stimulated for 15h at 37°C and 5% CO2 in the presence of anti-human CCR7. Following stimulation, cells were washed by PBS 1X, and stained for a viability dye (Aquavivid, Thermo Fisher scientific, Waltham, MA) for 20 min at room temperature in PBS. Cells were then stained for surface markers (CD3, CD4, CD45RA, CD27, CD57, CD14, CD19, CD8, CD28, PD-1, CD69, TIGIT, 4-1BB, ICOS, OX40, CD40L) for 30 min at 4°C, and fixed using 2% paraformaldehyde (Sigma-Aldritch, 15min, RT) before acquisition on a Symphony flow cytometer (BD Biosciences) and analyzes using FlowJo BD v10.8.1 software. For total PBMCs conditions, a CD40 blocking antibody (Miltenyi) was added in culture to prevent the interaction of CD40L with CD40 and its subsequent downregulation. Antibodies used are listed in Table S3.

Unsupervised clustering

Unsupervised analyses were performed on $CD4^+$ and $CD8^+$ T cells from UD, UNT, and ART donors that were activated by the aCD3:aCD28:IgG ratios of 1:0:4, 1:1:3, and 1:4:0. These data were first downsampled to an equal number of events (1,000 cells), and FCS files were loaded through the flowCore package (v2.10.0).[99] Scaling and logicle transformation of the flow cytometry data was applied using FlowSOM (v2.6.0),[100] as done previously.[52,101] The uniform manifold approximation and projection (UMAP) algorithm was performed using the R package M3C (v1.20.0),[102] while the clustering was achieved using Phenograph (v0.99.1)[56] with the k parameter (number of nearest-neighbors) set to 400. Cytokines were the only parameters used for clustering. Therefore, no cells were clustered based on the expression of any surface marker, such as CD4 and CD8. We obtained 17 clusters. All samples of $CD4^+$ and $CD8^+$ activated T cells by aCD3:aCD28:IgG

ratios of 1:0:4, 1:1:3, and 1:4:0, from the three cohorts (UD, UNT and ART) were loaded for clustering to form a single Multiparametric UMAP. The identification of T cell clusters relied solely on cytokine expression, and the phenotypic CD4 and CD8 information was reintroduced *post-hoc* using categorical single-cell phenotypic information. Therefore, $CD4^+$ and $CD8^+$ T cells could be subsequently displayed separately. For example, in the first panel of Figure 3A (CD4 1:0:4), we only visualized $CD4^+$ T cells activated by an aCD3:aCD28:IgG ratio of 1:0:4. Heatmaps were also generated in R (v4.2.2) using the packages gglot2 (v3.4.0)[103] and pheatmap (v1.0.12).[104] To accommodate cytokines with rare expression, the heatmaps were scaled by individually normalizing the values of each cytokine between 0 and 1, using their respective minimum and maximum values. The R code scripted for this paper is available at "original code: https://github.com/alemi055/scripts-and-data/blob/master/ShaabanKabakiboetal_2024.R".

QUANTIFICATION AND STATISTICAL ANALYSIS

Statistical analyses

Symbols represent biologically independent samples from UD, UNT and ART donors. Lines connect data from the same donor. Differences in responses for the same patient before and after ART treatment or from different activation conditions were assessed using Wilcoxon matched-pair tests. Differences in responses between UD and UNT were measured by Mann-Whitney tests. Wilcoxon and Mann-Whitney tests were generated using GraphPad Prism (version 9.2.0). p values < 0.05 were considered significant. p values are indicated for each comparison assessed. For graphical representation on a log scale (but not for statistical tests), null values were arbitrarily set at the minimal values for each assay.